Circulating extracellular vesicle microRNAs mediate immune modulation of social behavior in mice

Ken Matoba[1,8], Eisuke Dohi[1,2,7,8], Phoebe A. Garcia[1,8], Jose Francis-Oliveira[1,8], Mirmohammadali Mirramezanializamini[1], Inssaf Berkiks[1], Frida Anguiano[1], Jana H. Badrani[1], Oluwaseun Fatoba[1], Eric Y. Choi[2], Julia See[2], Md. Sorwer Alam Parvez[1], Takahiro Kochi[1], Norimichi Ito[1], Rei Mitani[2], Indigo V.L. Rose[2], Takashi Imai[2], David K. Crossman[3], Mikhail V. Pletnikov[2,6], Kenneth W. Witwer[4], Minae Niwa[1,2,5], and Shin-ichi Kano[1,2,5]*

[1]Department of Psychiatry and Behavioral Neurobiology, University of Alabama at Birmingham Heersink School of Medicine, Birmingham, AL, USA

[2]Department of Psychiatry and Behavioral Sciences, Johns Hopkins University School of Medicine, Baltimore, MD, USA

[3]Department of Genetics, University of Alabama at Birmingham Heersink School of Medicine, Birmingham, AL, USA

[4]Departments of Molecular and Comparative Pathobiology and Neurology, and The Richman Family Precision Medicine Center of Excellence in Alzheimer's Disease, Johns Hopkins University School of Medicine, Baltimore, MD, USA

[5]Department of Neurobiology, University of Alabama at Birmingham Heersink School of Medicine, Birmingham, AL, USA

[6]Present address: Department of Physiology and Biophysics, Jacobs School of Medicine and Biomedical Sciences, SUNY University at Buffalo, Buffalo, NY, USA

[7]Present address: National Institute of Neuroscience, National Center of Neurology and Psychiatry, Tokyo, Japan

[8]These authors equally contribute to this work.

*Correspondence should be addressed to S.K. (sikano@uabmc.edu)

Abstract

Extracellular vesicles (EVs) are cell-derived small membrane vesicles and circulate throughout the body, but the impact of circulating EVs on brain function and behavior remains elusive. Here, we report that wild-type (WT) mouse blood, particularly EVs, increases sociability in socially impaired immunodeficient *Rag1*$^{-/-}$ mice, mimicking the effects of WT T cell transfer. These EVs localized to neurons and regulated PKCε expression, $GABA_A$ receptor synaptic localization, and inhibitory postsynaptic signaling in prefrontal cortex (PFC) pyramidal neurons. Injection of *Rag1*$^{-/-}$ EVs supplemented with miR-23a-3p and miR-103-3p enhanced synaptic function and sociability in *Rag1*$^{-/-}$ mice. T cells secreted miR-23a-3p via EVs, and *Mir23a*$^{-/-}$ T cells failed to increase sociability. Similar beneficial effects of WT blood EVs were observed in additional mouse models with sociability deficits, *Cntnap2*$^{-/-}$ and *Shank3*$^{-/-}$ mice. These findings uncover a previously unrecognized role of EV miRNAs in mediating immune modulation of synaptic function and social behavior, revealing a novel molecular pathway for immune-neuron communication.

Introduction

Factors circulating in the blood can influence brain function and behavior in rodents. An emerging concept in aging research is that the transfusion of young rodent blood into aged rodents enhances memory function [1, 2]; however, it is unclear whether normal blood components ameliorate other behavioral deficits in a non-aging context. Accumulating evidence supports the requirement of lymphocytes, such as T cells, for brain function and behavior. Notably, immunodeficient mice, lacking T and B cells, display deficits in various behaviors, such as learning and memory, anxiety-related behaviors, and social behaviors [3-6]. Although T cell-derived cytokines, such as interferon-gamma (IFN-γ), interleukin-4 (IL-4), and IL-17, have been shown to influence these behaviors [4, 5, 7], additional factors may be involved in immune regulation of brain function and behavior. Indeed, lymphocytes have been shown to affect gut microbiota-derived metabolites, glucocorticoids, amino acids, and extracellular microRNAs (miRNAs) in the blood [6, 8-10].

Here, to further address the influence of circulating blood components on brain function and behavior, we examined the effects of a blood transfusion on social behaviors using immunodeficient mice. We discovered that intravenous injection of extracellular vesicles (EVs) from wild-type (WT) mouse blood, as well as WT mouse blood transfusion, improved in sociability but not social novelty preference in immunodeficient *Rag1*$^{-/-}$ mice. WT blood EVs modulate inhibitory postsynaptic currents (IPSCs) in the medial prefrontal cortex (mPFC) via miRNA-mediated control of gene expression. We identified T cells as the source of EVs and miRNAs that influence synaptic function and sociability. Notably, WT blood EVs also increased sociability and IPSC in two additional mouse models, *Cntnap2*$^{-/-}$ and *Shank3*$^{-/-}$ mice, highlighting a potential shared mechanism. Therefore, we have identified a previously unrecognized role of circulating blood EVs on brain function and behavior.

Results

Intravenous injection of WT serum enhances sociability in immunodeficient *Rag1*$^{-/-}$ mice. Previous studies reported that immunodeficient *scid* and *Rag2*$^{-/-}$ mice, lacking T and B cells, showed sociability deficits in the three-chamber social interaction test [5, 11]. Consistent with these findings, we observed that *Rag1*$^{-/-}$ mice also exhibited sociability deficits in this assay (**Fig. 1a, b**), despite normal performance in olfaction function or open field exploration (**Supplementary Fig. 1a, b**). To determine whether immune cell reconstitution could beneficially impact sociability, we performed adoptive transfer of splenocytes or purified T cells from WT mice into *Rag1*$^{-/-}$ mice. Both transfers significantly increased sociability in *Rag1*$^{-/-}$ mice (**Fig. 1c, d,** and **Supplementary Fig. 2a, b**). This suggests that the behavioral deficits were due to the absence of T and B cells, as Rag1 protein was undetectable in the brain during prenatal development, early postnatal stages, and adulthood (**Supplementary Fig. 1c, d**). Remarkably, intravenous injection of serum from WT mice also increased sociability in *Rag1*$^{-/-}$ mice (**Fig. 1e**). Although circulating cytokines such as IFN-γ and IL-17 were shown to modulate social behavior [5, 7], their concentrations in WT serum were extremely low - below the detection limit of the enzyme-linked immunosorbent assay (**Supplementary Fig. 2c**). These findings suggest that other circulating factors in WT blood may mediate the observed behavioral improvement. Therefore, we sought to identify additional blood components that might regulate sociability.

T cell-dependent improvement in sociability by *Rag1*$^{-/-}$ mice is associated with changes in EV-associated miRNAs in the blood.

Extracellular vesicles (EVs) are nanosized, membrane-enclosed vesicles that carry diverse cell-derived molecular cargo, such as RNAs, proteins, lipids, and carbohydrates [12-14]. Secreted by virtually all cell types, EVs are involved in waste disposal, antigen presentation, and intercellular communication [12-17]. Once released into circulation, EVs can reach distant organs and modulate their function [18, 19]. Circulating EV-associated molecules, particularly those of brain origin, have

emerged as promising biomarkers in neurological and psychiatric disorders, including Alzheimer's disease, psychotic disorders, depression, and autism spectrum disorders (ASDs) [20-32]. Moreover, several studies suggest that circulating EVs negatively impact brain function and behavior under disease conditions [23, 32, 33]. Nevertheless, whether and how circulating EVs and their molecular cargo influence brain function and behavior remains unknown.

To determine whether EVs contribute to the behavioral improvement by WT serum, we collected blood EVs (hereafter bEVs) from WT and *Rag1*$^{-/-}$ sera. Although the morphology, size distribution, and concentration of bEVs were comparable between WT and *Rag1*$^{-/-}$ mice, we observed reduced expression of an EV marker CD9 in *Rag1*$^{-/-}$ bEVs (**Supplementary Fig. 3a-f**). CD3ε protein in bEVs, likely derived from T cells, was also significantly diminished in *Rag1*$^{-/-}$ mice (**Supplementary Fig. 3f**). Thus, *Rag1*$^{-/-}$ bEVs are qualitatively altered and lack T cell-derived EVs. Adoptive transfer of WT T cells, which increased sociability (**Fig. 1d**) and the expression levels of CD3ε protein and miRNAs in *Rag1*$^{-/-}$ bEVs (**Fig. 1f, g** and **Supplementary Table 1**). Notably, the differentially expressed miRNAs significantly overlapped with those altered in multiple mouse models exhibiting sociability deficits (**Fig. 1h**). Predicted target genes of these miRNAs were enriched for pathways related to neuronal and synaptic function (**Fig. 1i** and **Supplementary Table 2-4**). These findings suggest that T cell-derived EVs and their miRNAs cargo may modulate sociability by influencing synaptic gene expression in the brain.

WT blood EV transfer improves sociability in *Rag1*$^{-/-}$ mice without affecting social novelty preference.

To directly assess the impact of circulating EVs on social behavior, we intravenously injected WT bEVs into *Rag1*$^{-/-}$ mice (**Fig. 2a**). WT EV injection did not change the numbers of peripheral T or B cells (**Supplementary Fig. 4**) but significantly increased sociability in *Rag1*$^{-/-}$ mice (**Fig. 2b**, and **Supplementary Fig. 5a**). Notably, WT bEVs also increased sociability in *Cntnap2*$^{-/-}$ and

Shank3$^{-/-}$ mice, two established mouse models of sociability deficits (**Fig. 2c, d**). In contrast, WT bEVs had no effect on sociability in WT mice (**Fig. 2e**), excluding the possibility that a mere increase in circulating EVs may enhance sociability. *Rag1*$^{-/-}$ mice also exhibited deficits in social novelty preference in the three-chamber social interaction test (**Fig. 2f, g**). However, WT bEVs did not improve social novelty preference in these mice (**Fig. 2h** and **Supplementary Fig. 5b**), indicating a selective effect on neuronal function underlying sociability. Consistently, the transfer of either WT sera, splenocytes, or T cells also failed to increase social novelty preference in *Rag1*$^{-/-}$ mice (**Supplementary Fig. 5c, d**). Together, these findings demonstrate that WT bEVs selectively improve sociability, but not social novelty preference, in *Rag1*$^{-/-}$ mice.

Circulating bEVs reach the brain parenchyma and co-localize with neurons and microglia in *Rag1*$^{-/-}$ mice.

To gain insight into the mechanisms underlying sociability improvement by WT bEVs, we examined their distribution in the brain following intravenous injection. WT bEVs were first labeled with a lipophilic dye, PKH26, and intravenously injected into *Rag1*$^{-/-}$ mice. As early as 1 hour post-injection, labeled bEVs were detected throughout the brain, including the medial prefrontal cortex (mPFC), the hippocampus, and the cerebellum (**Fig. 3a, b**). As lipid dye labeling may be promiscuous and generate non-EV micelles [34], we validated these findings using bEVs collected from mTmG mice, which express a membrane-anchored tdTomato fluorescent protein [35]. Consistent with the PKH26 labeling, tdTomato-positive bEVs were detected in the mPFC of *Rag1*$^{-/-}$ mice (**Fig. 3c**). Cell-type-specific analysis revealed that WT bEVs co-localized with neurons and microglia, but not with astrocytes or oligodendrocytes (**Fig. 3d, e** and **Supplementary Fig. 6a, b**), suggesting that these cell types may be primary recipients of circulating EVs in the brain.

WT bEVs improve sociability by attenuating hyperexcitability in the mPFC.

The mPFC plays a crucial role in the control of sociability behaviors [36-39]; hence we determined its involvement in sociability deficits and their improvement by WT bEVs in *Rag1*$^{-/-}$ mice. We first examined neuronal activities using c-Fos protein expression, an indicator of neuronal activity. c-Fos expression in the mPFC was increased in *Rag1*$^{-/-}$ mice, mostly in CaMKIIα^{+} excitatory neurons, compared to WT mice (**Fig. 4a, b**, and **Supplementary Fig. 7a, b**). To address the causal role of the increased activity of CaMKIIα^{+} neurons in sociability deficits in *Rag1*$^{-/-}$ mice, we then conducted chemogenetic inhibition using an inhibitory DREADD (designer receptors exclusively activated by designer drugs), hM4D(Gi) [40]. Expression of hM4D(Gi) via adeno-associated virus (AAV) vectors [AAV-CaMKIIα-hM4D(Gi)-mCherry] in the mPFC CaMKIIα^{+} neurons increased sociability in *Rag1*$^{-/-}$ mice upon the intravenous injection of a DREADD agonist, clozapine *N*-oxide (CNO) (**Fig. 4c,** and **Supplementary Fig. 8a-d**). Notably, intravenous injection of WT bEVs reduced the mPFC c-Fos expression in *Rag1*$^{-/-}$ mice (**Fig. 4d, e**), suggesting that WT bEVs normalize mPFC excitability. These data indicate that WT bEVs increase sociability in *Rag1*$^{-/-}$ mice, at least in part, by attenuating the mPFC hyperexcitability.

WT bEVs restore inhibitory postsynaptic activities in the mPFC.

We next used whole-cell patch clamp recordings in brain slices to assess the impact of WT bEVs on synaptic activities in the mPFC. *Rag1*$^{-/-}$ mice exhibited significantly reduced amplitudes of spontaneous inhibitory postsynaptic currents (sIPSCs) compared to WT mice (**Fig. 5a, b**), while sIPSC frequencies showed a trending decrease. AMPA receptor-mediated spontaneous excitatory postsynaptic currents were unchanged between WT and *Rag1*$^{-/-}$ mice (**Supplementary Fig. 9a, b**). Notably, incubation of *Rag1*$^{-/-}$ brain slices with WT bEVs restored sIPSC amplitudes to WT levels (**Fig. 5a, b**). These findings suggest that impaired inhibitory postsynaptic signaling contributes to the mPFC hyperexcitability in *Rag1*$^{-/-}$ mice and is targeted by WT bEV. A similar beneficial effect was observed in *Cntnap2*$^{-/-}$ mice (**Fig. 5c, d**), indicating

that modulation of mPFC inhibitory postsynaptic signaling by WT bEV may be a shared mechanism underlying sociability improvement.

PFC transcriptomes change in *Rag1*$^{-/-}$ mice and by WT bEV administration.

To gain insight into the molecular mechanisms underlying EV-mediated modulation of mPFC neuronal activities, we performed RNA-seq analysis of the PFC of *Rag1*$^{-/-}$ mice following intravenous injection of WT bEVs. We also compared the PFC gene expression profiles between WT and *Rag1*$^{-/-}$ mice. WT bEV injection altered the expression of 2,027 genes in the *Rag1*$^{-/-}$ PFC (**Fig. 5e** and **Supplementary Tables 5-8**). Of these, 1,280 genes overlapped with the 4,772 genes differentially expressed between WT and *Rag1*$^{-/-}$ PFC (**Fig. 5f** and **Supplementary Table 9**). Pathway analysis revealed that these genes were enriched for synaptic regulation (**Fig. 5f** and **Supplementary Table 10**), indicating that WT bEVs modulate synapse-related gene expression in the *Rag1*$^{-/-}$ mPFC.

Small RNAs mediate sociability rescue by WT bEVs in *Rag1*$^{-/-}$ mice.

EV-associated miRNAs (EV miRNAs) have been shown to influence gene expression in recipient cells, even in a distant organ [14, 15, 18]. To test whether miRNAs mediate the behavioral and synaptic effects of WT bEVs, we first extracted small RNA factions from WT bEVs and loaded them into *Rag1*$^{-/-}$ bEVs, as previously described [41]. These reconstituted bEVs (*Rag1*$^{-/-}$ bEVs + WT RNA) were intravenously injected into *Rag1*$^{-/-}$ mice. Sociability was then compared with *Rag1*$^{-/-}$ mice receiving *Rag1*$^{-/-}$ bEVs + *Rag1*$^{-/-}$ RNA and WT bEVs + WT RNA. *Rag1*$^{-/-}$ mice receiving *Rag1*$^{-/-}$ bEVs + WT RNA showed significantly enhanced sociability, comparable to those receiving WT bEVs + WT RNA and higher than those receiving *Rag1*$^{-/-}$ bEVs + *Rag1*$^{-/-}$ RNA (**Supplementary Fig. 10a, b**). These findings demonstrate that small RNAs associated with WT bEVs, most likely miRNAs, are sufficient to rescue sociability in *Rag1*$^{-/-}$ mice.

***Rag1*$^{-/-}$ mice show altered expression of miR-23a-3p and miR-103-3p in bEVs and their predicted target, PKCε, in the mPFC.**

To identify the miRNA cargo and their target mRNA by which WT bEVs increase sociability and modulate mPFC neuronal activities, we further analyzed our EV miRNA-seq (**Fig. 1g** and **Supplementary Table 1**) and PFC RNA-seq datasets (**Fig. 5e, f** and **Supplementary Tables 5-8**). We focused on 755 mRNAs that were upregulated in *Rag1*$^{-/-}$ PFC compared to WT and downregulated by WT bEV injection (**Fig. 6a** and **Supplementary Table 10**). These mRNAs were potential targets of WT bEV miRNAs that were reduced in *Rag1*$^{-/-}$ mice. As WT bEVs enhanced inhibitory postsynaptic activities in the mPFC of *Rag1*$^{-/-}$ mice (**Fig. 5a, b**), we prioritized mRNAs implicated in GABAergic synapse regulation and identified seven candidates (**Fig. 6a**). Comparing these mRNAs with predicted targets of the 40 miRNAs whose expression increased by WT T cell transfer in *Rag1*$^{-/-}$ bEVs (**Fig. 1g** and **Supplementary Tables 11-12**), we identified *Prkce*, encoding protein kinase C epsilon (PKCε), as a plausible target. PKCε has been shown to reduce GABA-mediated postsynaptic inhibitory currents by downregulating postsynaptic $GABA_A$ receptor localization [42]. We indeed found increased PKCε protein levels in the *Rag1*$^{-/-}$ mPFC neurons by immunohistochemistry (**Fig. 6b, c**). Consistent with a previous study reporting that PKCε downregulates synaptic $GABA_A$ receptor levels [42], we observed that synaptic $GABA_A$ receptor localization [$GABA_A$ receptor subunit ($GABA_A$Rγ2) associated with Gephyrin] on CaMKIIα$^+$ neurons decreased in the *Rag1*$^{-/-}$ mPFC (**Fig. 6d, e**). We also observed that two miRNAs predicted to target PKCε, miR-23a-3p and miR-103-3p (**Supplementary Fig. 11a**), were present in WT bEVs but significantly reduced in *Rag1*$^{-/-}$ bEVs (**Fig. 6f**). Notably, miR-23a-3p was also downregulated in bEVs from *Shank3*$^{-/-}$ and *Cntnap2*$^{-/-}$ mice (**Supplementary Fig. 11b**). These findings suggest that WT bEV-associated miRNAs, particularly miR-23a-3p and miR-103-3p, modulate mPFC inhibitory postsynaptic signaling by regulating PKCε expression and synaptic $GABA_A$ receptor localization.

Intravenous injection of *Rag1*$^{-/-}$ bEVs loaded with miR-23a-3p and miR-103-3p increases sociability and reduces mPFC hyperexcitability.

We next tested whether miR-23a-3p and miR-103-3p could impact the mPFC neuronal alterations and increase sociability deficits in *Rag1*$^{-/-}$ mice. We loaded *Rag1*$^{-/-}$ bEVs with miRNA mimics of miR-23a-3p and miR-103-3p and intravenously injected them into *Rag1*$^{-/-}$ mice (**Fig. 7a**). *Rag1*$^{-/-}$ mice receiving these reconstituted bEVs significantly improved sociability compared to those receiving *Rag1*$^{-/-}$ bEVs loaded with non-targeting control mimics (**Fig. 7b**). The behavioral improvement was accompanied by reduced expression of neuronal c-Fos and PKCε, and increased levels of synaptic $GABA_A$ receptor in the mPFC (**Fig. 7c-h**). Finally, brain slice electrophysiology revealed that *Rag1*$^{-/-}$ bEVs loaded with miR-23a-3p and miR-103-3p significantly enhanced sIPSC amplitudes in the mPFC pyramidal neurons compared to *Rag1*$^{-/-}$ bEVs loaded with non-targeting control mimics (**Fig. 7i, j**). These data indicate that miR-23a-3p and miR-103-3p are key mediators of bEV-induced improvement of sociability and mPFC inhibitory neurotransmission through regulation of PKCε and synaptic $GABA_A$ receptor (**Fig. 7k**).

miR-23a-3p in T cell-derived EVs contributes to sociability.

We finally examined the source of pro-social EV miRNAs, miR-23a-3p and miR-103-3p. First, we excluded the possibility that these miRNAs were merely co-precipitated with EVs during bEV collection. As EV miRNAs are protected from RNase degradation unless the vesicle membrane is disrupted (e.g., by Trixon-X100 treatment) [43, 44], we treated bEVs with RNase in the presence or absence of 1% Triton-X100. Levels of miR-23a-3p and miR-103-3p were reduced only in the presence of 1% Triton-X100 (**Supplementary Fig. 12a, b**), indicating that these miRNAs are primarily located inside the EVs, although a fraction may be on the surface.

We then investigated the cellular origin of these miRNAs. Since T cell transfer into *Rag1*$^{-/-}$ mice increased their levels in bEVs (**Fig. 1f**), we tested whether T cells secrete EVs containing these

miRNAs. T cells were purified from spleens, cultured, and EVs were collected from the conditioned medium (**Fig. 8a**). Notably, miR-23a-3p and, at a lesser level, miR-103-3p were detected in T cell-derived EVs (**Fig. 8b** and **Supplementary Fig. 13a**). Following intravenous injection into *Rag1*$^{-/-}$ mice, these cultured T cell-derived EVs were detected in the mPFC and co-localized with neurons and microglia (**Fig. 8c, d**, and **Supplementary Fig. 13b**), similar to the whole bEVs (**Fig. 3**) and *in vivo* generated T cell-derived EVs (**Supplementary Fig. 13c-f**), supporting their physiological relevance.

We finally determine whether T cell-derived miR-23a-3p contributed to the effects of WT bEVs on sociability using *Mir23a*$^{-/-}$ mice [45]. *Mir23a*$^{-/-}$ bEVs failed to restore sIPSC amplitudes in the PFC of *Rag1*$^{-/-}$ and *Cntnap2*$^{-/-}$ mice (**Supplementary Fig. 14a, b**), consistent with the role of miR-23a-3p in mPFC inhibitory neurotransmission (**Fig. 7i, j**). We purified T cells from *Mir23a*$^{-/-}$ mice and compared their ability to influence sociability deficits in *Rag1*$^{-/-}$ mice with that of WT T cells (**Fig. 8e**). Despite successful T cell reconstitution (**Fig. 8f, g**), *Rag1*$^{-/-}$ mice receiving *Mir23a*$^{-/-}$ T cells exhibited reduced levels of miR-23a-3p in bEVs (**Fig. 8h**), indicating that T cells are a major source of this miRNA in circulating EVs. Remarkably, adoptive transfer of *Mir23a*$^{-/-}$ T cells failed to increase sociability in *Rag1*$^{-/-}$ mice (**Fig. 8i**). Together, these findings demonstrate that miR-23a-3p is secreted in EVs from T cells and contributes to sociability.

Discussion

This study reveals that T cell-derived EV miRNAs in circulating EVs regulate sociability in mice. We demonstrated that circulating EVs enter the brain parenchyma and co-localize with neurons and microglia in the mPFC. At the molecular level, EV miRNAs, particularly miR-23a-3p and miR-103-3p, reduce PKCε expression, enhance synaptic $GABA_A$ receptor localization, and increase inhibitory postsynaptic signaling in the *Rag1*$^{-/-}$ mPFC pyramidal neurons. We further identified miR-23a-3p and miR-103-3p in T cell-derived EVs that co-localize with neurons in the

mPFC. Notably, *Mir23a*$^{-/-}$ T cells failed to increase sociability in *Rag1*$^{-/-}$ mice and *Mir23a*$^{-/-}$ bEVs did not enhance sIPSC in *Rag1*$^{-/-}$ mPFC pyramidal neurons. Beneficial effects of WT bEVs were also observed in *Cntnap2*$^{-/-}$ and *Shank3*$^{-/-}$ mice, and *Mir23a*$^{-/-}$ bEVs were unable to increase sIPSC in *Cntnap2*$^{-/-}$ mice, implicating miR-23a-3p loss as a shared mechanism underlying inhibitory synaptic dysfunction in the mPFC across models of sociability deficits. Therefore, our findings provide novel conceptual and mechanistic insights into how circulating T cell-derived EV miRNAs influence brain synaptic activity and sociability, and suggest that EVs and miRNAs may have therapeutical potential for sociability impairment.

PKCε has been shown to downregulate synaptic $GABA_A$ receptors via the N-ethylmaleimide-sensitive factor and reduce inhibitory postsynaptic currents in the hippocampus [42]. Our study shows that PKCε-dependent modulation of GABAergic signaling is also critical in the mPFC, where its dysregulation leads to neuronal hyperexcitability. This modulation is further regulated by circulating EV-associated miRNAs, miR-23a-3p and miR-103-3p. Considering that blood EVs are also detected in the hippocampus and cerebellum, similar EV miRNA-mediated modulation of synaptic neurotransmission may occur in other brain regions. Previous studies have reported that local protein translation controls the expression of $GABA_A$ receptors and some PKC isoforms [46-48]; thus, EV miRNAs may directly influence the local translation of PKCε at synapses, regulating synaptic $GABA_A$ receptor level. It remains unclear whether and how the expression changes in a pleiotropic enzyme, PKCε, preferentially influence GABAergic signaling in the mPFC. As the current knowledge of predicted targets by miRNAs is still limited, we cannot completely exclude that miR-23a-3p and miR-103-3p may regulate GABAergic signaling via molecules other than PKCε.

While earlier studies have focused on the role of cytokines, canonical effector molecules of T cells, in regulating neuronal activity and behavior [4, 5, 7, 49], our data uncover a previously

unrecognized role for miRNAs. Specifically, we identify miR-23a-3p and miR-103-3p as pro-social EV miRNAs derived from T cells. T cell-derived EVs and their miRNAs are known to modulate immune cell function [50, 51], but their role outside the context of immune responses has been largely unexplored. Our findings establish a new paradigm that miRNAs mediate immune cell communication with neurons in a more physiological context. Our study also defines T cells as an important source of circulating EVs and miRNAs that mediate the blood-brain communication regulating neuronal function and behavior. Future studies will determine which T cell subsets (e.g., $CD4^+$ T cells, γδ T cells) contribute to pro-social EV miRNA production. Currently, the lack of cell type-specific EV markers limits our ability to trace specific EVs in circulation back to their cellular origin, but such challenges will be overcome soon with rapid advances in EV research.

The EV uptake by brain cells was selective. We observed substantial overlaps of bEV signals with neurons and microglia, but not astrocytes or oligodendrocytes. As macrophages are known to take up EVs in the periphery and circulation [52, 53], microglial uptake of bEVs may not be surprising and is likely to be related to their homeostatic function. In contrast, neuronal uptake of bEVs is unexpected because neurons are not professional phagocytes. Although further research is required, bEV uptake by neurons may depend on some specific mechanisms (e.g., receptors for certain EV surface proteins) and be selective for certain types of EVs (e.g., EVs with surface protein modifications).

Notably, the behavioral improvement was also selective. WT bEVs improved sociability but not social novelty preference in *Rag1*$^{-/-}$ mice. Similarly, WT serum, splenocytes, and T cells failed to improve social novelty preference. Thus, circulating T cell-derived EVs may preferentially target sociability-related neuronal circuitry, highlighting the significance of possible EV tropism for specific cell types or brain regions. One limitation of this study is the fact that the *Rag1*$^{-/-}$ mouse

sociability scores were variable across different experiments, which was likely caused by multiple factors, particularly the changes in mouse housing conditions and behavioral rooms, that we experienced during this study. However, our data consistently showed the improvement of sociability by WT bEVs, underscoring the beneficial effects of WT bEVs.

Intriguingly, we observed the beneficial effects of bEVs on sociability in *Cntnap2*$^{-/-}$ and *Shank3*$^{-/-}$ mice as well. Nevertheless, the underlying mechanisms have not been thoroughly dissected in the current study. Although we showed that bEVs improved electrophysiological phenotypes in a miR-23a-dependent manner in *Cntnap2*$^{-/-}$ mice, it remains unclear whether the PKCε-$GABA_A$ receptor axis is similarly impaired in these mice. It is also unclear whether the beneficial effects of bEVs on *Shank3*$^{-/-}$ mice are dependent on miR-23a-3p. Further studies are required to determine the common and selective mechanisms underlying the effects of WT bEVs on sociability across multiple mouse models.

Our findings are also consistent with previous human studies. Altered expression of miR-23a-3p and miR-103-3p has been reported in the brain tissues and blood of patients with autism spectrum disorders (ASD) and schizophrenia [54-57], conditions accompanied by sociability deficits. miR-23a-3p is decreased in the peripheral blood of patients with schizophrenia [55], while miR-103-3p is consistently decreased across multiple studies with ASD patients [56, 57]. Notably, one study also found that the miR-23a-3p targets genes related to synaptic function and ASD risks [54]. Nevertheless, the behavioral consequences of these miRNA changes remain unclear. Future studies should investigate whether the blood levels of miR-23a-3p and miR-103-3p correlate with sociability and other cognitive functions in these patients and may have therapeutic potentials as observed in multiple mouse models with sociability deficits in this study.

Finally, our work underscores the need to investigate blood EV changes not only as biomarkers but also as possible pathological mechanisms in psychiatric and neurological disorders[14, 58]. While blood EV alterations are recognized as useful biomarkers, our research indicates that they may also play crucial roles in disease mechanisms involving periphery-brain communication. Importantly, our work demonstrated that the supplementation of EVs and miRNAs improved sociability. Although engineering cell culture-derived EVs is currently a popular therapeutic approach, our findings suggest that modulating autologous circulating EVs and miRNAs may be another promising strategy to restore neuronal function and behaviors under pathological conditions.

Methods

Mice

Rag1$^{-/-}$, *Cntnap2*$^{-/-}$, and *Shank3*$^{-/-}$, mTmG, and C57BL/6 mice (Stock# 002216, 017482, 017688, 007676, and 000664) were purchased from the Jackson Laboratory and housed in specific pathogen-free facilities at the Johns Hopkins University and the University of Alabama at Birmingham. *Mir23a*$^{-/-}$ mice were obtained from Dr. Richard Dahl (Indiana University, USA). All the mice were on C57BL/6 background. Male mice were used for the experiments at 8–12 weeks of age unless stated otherwise. All experimental procedures were performed under the animal protocols approved by the Institutional Animal Care and Use Committees.

Behavioral assays

Behavioral assays were performed on male mice at 8-12 weeks of age. All the assays were conducted between 10 am and 3 pm during the light phase. Independent cohorts of mice were tested in the three-chamber social interaction test, the open field test, and the buried food pellet test.

Three-chamber social interaction test: The three-chamber social interaction test was conducted as previously described [59, 60]. All mice were tested in a nonautomated three-chambered box. Dividing walls had retractable doorways allowing access into each chamber. Mice were acclimated to the three-chambered box for 4 days before the test (10 min/day). On the test day, mice were transported to the testing room and habituated for at least 1 h before the experiment. A white noise generator was used to mitigate any unforeseen noises. The subject mouse was habituated in the chamber with two empty cylinders for 10 min. Then, the “toy” object was placed in one of the cylinders and mouse (stranger 1) was placed in another cylinder for the “sociability” trial. Mice were allowed to explore the chambers for 10 min. In the next “social novelty preference” trial, stranger 1 was kept in the cylinder as the familiar mouse and the toy object was replaced with a novel mouse (stranger 2). The subject mouse was again

allowed to explore the chambers. During these two trials, mouse activities were recorded on video and the time spent sniffing each cylinder was manually measured. Preference index was calculated as follows. For sociability test: (sniffing time to mouse) x 100 / (sniffing time to mouse + sniffing time to object) - 50. For social novelty preference test: (sniffing time to novel mouse) x 100 / (sniffing time to novel mouse + sniffing time to familiar mouse) - 50.

Buried food pellet test: The buried food pellet test was performed as previously described [61]. Mice were food-deprived for 24 h with free access to water. At the test, single mouse was placed in the test cage and allowed to freely explore the food pellets buried ~0.5 cm below the surface of a 3 cm-deep layer of beddings. Latency to find the hidden food pellet was measured. (n=11-18 mice per group).

Open field test: Novelty-induced activity in the open field was assessed as described previously [60, 62]. Locomotion, rearing, and center time were measured for 10 min using a Photobeam Activity System (PAS–Open Field, San Diego Instruments). The PAS system consisted of two vertically stacked frames, each containing infrared lasers arranged in a 16 x 16 grid, which detected mouse movement, including ambulation and rearing. The open field box and surrounding photobeam apparatus were housed in a ventilated cabinet. Single-beam breaks were automatically recorded as “counts” and the PAS system automatically started recording counts once the mouse started moving. The total counts were recorded and the percentages of center counts (defined as those in the central 27.5 x 27.5 cm area) to total counts were calculated.

Serum and EV preparation

Blood (600-700 µl) was collected from mice via cardiac puncture under a deep anesthesia at time of sacrifice and placed at room temperature for 30 min. Sera were then separated by centrifugation at 300 x *g* for 5 min and stored at -80ºC for biochemical/molecular experiments or freshly used for *in vivo* experiments. For EV preparation, the sera were further centrifuged with

2,000 x *g* 10 min to remove platelets. EVs were prepared primarily with differential ultracentrifugation (UC), except for **Supplementary Fig. 3 and 5** where precipitation (PPT) and size exclusion chromatography (SEC) were also used as indicated. For EV enrichment with differential ultracentrifugation, the sera were centrifuged at 10,000 x *g* for 30 min at 4ºC to remove large vesicles. Then, the sera were diluted with PBS at 1:4 ratio and ultracentrifuged at 100,000 x *g* for 30 min at 4ºC using Optima MAX-XP ultracentrifuge with a TLA 120.2 rotor (k factor = 11) (Beckman Coulter) [63]. The pellet was resuspended with 1 ml of PBS and ultracentrifuged at 100,000 x *g* for 30 min at 4ºC to wash, and then resuspended with 10 µL of PBS. For EV precipitation, the sera were processed with Total Exosome Isolation kit (Thermo Fisher Scientific) following the manufacturer's protocol and the EV-containing fraction was resuspended in 50 µL PBS. For EV enrichment with size exclusion chromatography, each serum sample was applied to a 70 nm qEVsingle size exclusion column (Izon) and eluted with DPBS. Fractions were collected using an Izon automated fraction collector: following elution of a 1-ml void fraction, 0.5-ml fractions were collected, of which fractions 6 to 8 were enriched in EVs. These fractions were pooled, concentrated using Amicon 15 Ultra RC 100 kD filters, and aliquoted and stored in LoBind tubes (Eppendorf) at -80°C.

Transmission Electron Microscopy

Freshly prepared EV samples were adsorbed onto carbon-coated/palladium grids for 1 min and negatively stained with 2% (w/v) uranyl acetate for 1 min. EVs were visualized under a FEI Tecnai Spirit T12 transmission electron microscope (Thermo Fisher Scientific / FEI).

Nano particle tracking analysis (NTA)

Concentration and size distribution of particles in EV samples were analyzed with NanoSight NS300 (Malvern Panalytical) or ZetaView (Particle Metrix) following standard protocols [64, 65].

Adoptive cell transfer, serum injection, and EV injection,

For adoptive cell transfer, splenocytes and T cells were collected from spleen. T cells were isolated using the Pan T cell isolation kit II, mouse (#130-095-130, Miltenyi Biotech). T cells were >99%-positive for CD3ε expression by flow cytometry. Splenocytes (1 x 10^8 cells 100 μL per mouse) and T cells (1 x 10^7 cells 100 μL per mouse) were transferred intravenously into *Rag1*$^{-/-}$ mice via retro-orbital injection following a standard protocol [66]. Sera (150 μL per mouse) and EVs (2 x 10^9 particle in 100 μL per mouse unless stated otherwise) were also transferred intravenously into WT and *Rag1*$^{-/-}$ mice via retro-orbital injection. In our method, the number of EVs recovered from 500 μL total venous blood was about 4 x 10^9 particles. Considering that the total blood volume of an adult mouse is 2 ml, our injection of 2 x 10^9 particles corresponds to about 12.5% volume of the total circulating EVs in the blood. This volume is less than the maximal blood volume (=13%) we can collect per single blood donation in humans [67, 68].

Primary T cell culture

Mouse primary T cells were purified from spleens as Thy1.2$^+$CD19$^-$ cells by FACS sorting with a BD FACSAria II and cultured following a standard protocol [66]. Briefly, purified T cells (1 x10^6 cells/ml per well on 24-well plates) were stimulated with plate-bound anti-CD3ε (1 μg/ml) and anti-CD28 (1 μg/ml) and cultured for 36 and 60 h in RPMI complete medium (RPMI, 10% FBS, 1% non-essential amino acids, 1% sodium pyruvate, 0.05 mM B-Mercaptoethanol, and 1% Pen/Strep). Cell culture supernatants were collected, and EVs were collected by UC as described above.

Western blot

EV and tissue lysates were prepared with RIPA buffer, separated on NuPAGE Bis-Tris Mini Gel (Thermo Fisher Scientific / Life Technologies) with equal amounts of total proteins loaded into

each lane, and transferred to PVDF membrane (Millipore). After blocking in 5% skim milk/PBS-0.1% Tween® 20 (PBS-T) for 1 h, the membrane was incubated with the primary antibody overnight at 4°C and then incubated with the HRP or fluorescent secondary antibodies for 1 h at room temperature. Chemiluminescence and fluorescence gel images were captured by ImageQuant LAS 4000 imager (GE Healthcare), Odyssey imaging system (Li-Cor Biosciences), and analyzed with ImageJ/Fiji software[4]. The following primary antibodies were used: rabbit anti-CD9 (1:1,000, #ab92726, Abcam, RRID: AB_10561589), rabbit anti-Alix (1:1,000, #ab186429, Abcam, RRID: AB_2754981), rabbit anti-Calnexin (1:1,000, #ADI-SPA-860-D, Enzo Life Science, RRID: AB_10616095), mouse anti-CD3ε (1:1,000, #362701, BioLegend, RRID: AB_2563713), armenian hamster anti-CD3ε (1:1,000, #100302, BioLegend, RRID: AB_312667), mouse anti-CD81 (1:1,000, #sc-166029, Santa Cruz Biotechnology, RRID: AB_2275892), armenian hamster anti-mouse CD81(1:1,000, #sc-18877, Santa Cruz Biotechnology, RRID: AB_627194), IRDye 680RD Donkey anti-mouse IgG(H + L) (1:10,000, LI-COR Biosciences #926-68072, RRID: AB_ 10953628), IRDye 800CW Donkey anti-rabbit IgG(H+L) (1:10,000, LI-COR Biosciences #926-32213, RRID: AB_621848), rabbit anti-Rag1 (1:1,000, #sc-5599, Santa Cruz Biotechnology, RRID: AB_2300670), mouse anti-Rag1 (1:1,000, #68591-1-Ig, Proteintech, RRID: AB_3085290), goat anti-Rag2 (1:1,000, #sc-7623, Santa Cruz Biotechnology, RRID: AB_2175836), rabbit anti-TNFα (1:1000, #17590-1-AP, Proteintech, RRID: AB_2271853), and mouse anti-β-actin (1:5,000, #sc-47778, Santa Cruz Biotechnology, RRID: AB_626632).

Flow cytometry

Flow cytometry of splenocytes was performed using a standard protocol [66]. Single cell suspensions were obtained from spleens collected after PBS perfusion. After lysis of red blood cell with 1x RBC Lysis Buffer (Thermo Fisher Scientific/eBioscience), cells were washed with FACS buffer and Fc-blocked with anti-CD16/CD32 (#14-0161-82, Thermo Fisher Scientific/eBioscience, RRID: AB_467133). Then, cells were stained with the following

antibodies: rat anti-CD3 APC (1:100, #100235 BioLegend, RRID: AB_2561455), rat anti-mouse CD19 PE (1:100, #115508, BioLegend, RRID: AB_313643), rat anti- B220 Alexa Fluor 488 (1:100, #103228, BioLegend, RRID: AB_492874), rat anti-mouse CD3 Alexa Fluor 488 (1:100, #100210, BioLegend, RRID: AB_ 389301), and rat anti-mouse CD45 FITC (1:100, #110705, BioLegend, RRID: AB_ 313494). Flow cytometry was conducted using FACS Calibur, LSRII, or Accuri C6 cytometer (all from BD Biosciences) and analyzed with FlowJo software (FlowJo LLC).

DREADD experiments

Mice were stereotactically injected with 400 nl of pAAV-CamKIIα-hM4D(Gi)-mCherry ($4.4x10^{12}$ genomic copies/mL, #50477, Addgene) at the rate of 100 to 200 nl/min into the mPFC bilaterally using a NanoFil syringe with a 35G blunt needle (WPI). The following stereotactic coordinate was used for injection; anteroposterior (AP): +1.8mm; mediolateral (ML): ± 0.3mm; and dorsoventral (DV): -2.1 mm from the bregma. Three to four weeks later, behavioral assays were conducted. CNO (10 mg/kg in 0.5% DMSO/PBS, #BML-NS105-0025, Enzo Life Sciences) was intraperitoneally injected 45 min prior to the three-chamber social interaction test. For the three-chamber social interaction test, mice were intraperitoneally injected with PBS during acclimation for 4 consecutive days and then injected with CNO or vehicle (0.5% DMSO/PBS) on the test day as previously described[69].

Brain collection

Mice were anesthetized and transcardially perfused with ice-cold PBS. For RNA-seq experiments, brains were dissected and stored at -80 ºC until use. For immunohistochemistry, mice were further perfused by 4% paraformaldehyde (PFA) and the dissected brains were fixed in ice-cold 4% PFA/PBS for 24 h.

Immunohistochemistry

Immunohistochemistry experiments were conducted as previously described [60, 70]. Free floating coronal sections (40 μm in thickness) were prepared with a Leica cryostat and, if necessary, antigen retrieval was performed with 10 mM sodium citrate buffer (pH8.5). The sections were then placed in blocking solution (PBS supplemented with 2% Normal Goat Serum, 1% BSA, 0.1% TritonX, 0.05% Tween-20, and 0.05% sodium azide) for 1 h at room temperature and then incubated at 4°C overnight with the following primary antibodies: mouse anti-NeuN (1:500, #MAB377, Merck-Millipore, RRID: AB_2298772), rabbit anti-Iba1 (1:400, #019-19741, Wako Chemicals, RRID: AB_839504), goat anti-c-Fos (1:500, #sc-52, Santa Cruz Biotechnology, RRID: AB_2106783), rabbit anti-c-Fos (1:200, #2250, Cell Signaling, RRID: AB_22472111), mouse anti-CaMKIIα (1:200, #688602, Clone 6G9, BioLegend, RRID: AB_2617027), rabbit anti-CaMKIIα (1:100, #20666-1-AP, Proteintech, RRID:AB_2878722), rabbit anti-RFP (1:1,000, #600-401-379, Rockland, RRID: AB_2209751), rabbit anti-PKCε (1:100, #20877-1-AP, Proteintech, RRID:AB_10697812), mouse anti-CC1 (1:100, #OP80, Calbiochem, RRID:AB_2057371), rabbit anti-S100β (1:200, #ab868, Abcam, RRID:AB_306716), mouse anti-NSE (1:500, #66150-1-g, Proteintech, RRID:AB_2881546), mouse anti-Gephyrin (1:100, #147021, Synaptic Systems, RRID:AB_2232546), and rabbit anti-$GABA_A$Rγ2 (1:100, #AGA-005, Alomone Labs, RRID: AB_2039870). After washing with PBS, the sections were further incubated with fluorophore-conjugated secondary antibodies at 1:400 dilution for 2 h at room temperature, followed by DAPI staining (1:50,000, #10236276001, Roche) for 10 min at room temperature. were used for signal detection. The sections were mounted on glass slides with Permafluor™ mounting medium or ProLong Diamond antifade mounting medium (Thermo Fisher Scientific). Images were acquired using Zeiss LSM510, 700 and 800 confocal microscopes with Zen software (Carl Zeiss) or an Olympus BX61 epifluorescence microscope (Olympus).

EV labeling and brain distribution analysis

For chemical dye labeling of EVs, WT EVs were stained with PKH26 lipophilic dye (Sigma-Aldrich). Briefly, EVs were suspended with 194 µl of Diluent C, mixed with 6 µl of PKH26 dye, and incubated for 5 min at room temperature. The reaction was stopped by adding 100 µl of 20% BSA. Then, the EV suspensions were applied to the Exosome Spin Column (Thermo Fisher Scientific) and spun down to remove excess amount of the dye. Next, stained EVs were diluted to 2 x 10^{10}/mL with DMEM medium (Thermo Fisher Scientific). For genetically labeling of EVs, EVs were collected from the sera of mTmG mice, in which cellular membranes and thus cell-derived EVs are labeled with membrane-anchored tdTomato. EVs (2 x 10^9 particles /mouse) were intravenously injected into recipient mice. Brains were collected 1 h later and PKH26 and tdTomato puncta were analyzed by immunohistochemistry.

Image analysis

Image analysis was performed as previously described [60]. c-Fos quantification was conducted using Image J/Fiji software[71] and the percentages of c-Fos-expressing cells among NeuN neurons were calculated. Images were taken at 20x and 40x magnification. The maximal projection images of z-stacked images (14 sections at 0.75 µm) were used for quantification with confocal. Three to five brain sections from each animal were chosen based on anatomic landmarks to ensure that equivalent regions were analyzed. EV co-localization images with each cell type marker (NSE^+, $Iba1^+$, $S100\beta^+$, and $CC1^+$ cells) were taken with 63x magnification. The maximal projection images of z-stacked images (14 sections at 0.34 µm) were used for quantification. The co-localization was defined when at least one EV puncta were overlapped with the cell marker staining. The percentages of EV-positive cells among all the cells for each cell type was quantified per visual field and averaged across 4-5 independent fields to calculate %EV-positive cells/total cells. The number of EVs was measured using ImageJ software as follows. Images of 1024x1024 pixels were taken with 63x magnification and

converted to 8-bit monochromes using "Split Channel" function. The number of EVs per field was calculated by counting particles between 3.5 and 10 pixels² using the "Analyze Particles" function, after setting the threshold to -50. For synaptic GABA receptor quantification, images were taken using a 63x magnification objective with 2x optical zoom. The maximal projection images of z-stacked images (14 sections at 0.34 μm) were used for quantification. Postsynaptic $GABA_AR\gamma2$ was determined by the co-localized puncta of $GABA_AR\gamma2$ and gephyrin on the soma of $CaMKII\alpha^+$ neurons. The number of $GABA_AR\gamma2^+$ $gephyrin^+$ puncta per $CaMKII\alpha^+$ neurons was counted and averaged across 5-6 $CaMKII\alpha^+$ neurons per mouse.

RNA-seq

Total RNAs were extracted from frontal cortices of mice transcardially perfused with ice-cold PBS using RNeasy micro kit (Qiagen). Libraries were prepared with NEB Next Ultra II Directional RNA Library Prep kit (New England BioLabs) and a 75-bp paired-end sequencing was performed on a NextSeq500 (Illumina) at the UAB Genomics Core. Raw RNA sequencing reads were aligned to the mouse reference genome (GRCm38 p6, Release M24) from Gencode with STAR (version 2.7.5c) (using parameters --outReadsUnmapped Fastx --outSAMtype BAM SortedByCoordinate --outSAMattributes All)[72]. Following alignment, HTSeq-count (version 0.12.3) was used to count the number of reads mapping to each gene (using parameters -r pos -t exon -i gene_id -a 10 -s no -f bam)[73]. Normalization and differential expression were then applied to the count files using DESeq2 (version 1.28.1) following their vignette[74]. Lists were compiled of genes whose expression was significantly altered between *Rag1*$^{-/-}$ mice and WT mice, and between *Rag1*$^{-/-}$ mice with and without WT EVs. P values were adjusted using the Benjamini-Hochberg false discovery rate (FDR) and the adjusted $p < 0.05$ was considered statistically significant. Then, genes whose expression changes were overlapped were extracted for the downstream analysis. Gene ontology (GO) enrichment analysis was performed

using Metascape[75], including biological process (BP), molecular function (MF) and cellular component (CC).

miRNA-seq

Total RNAs containing small RNA fractions were extracted from EVs enriched with differential ultracentrifugation using miRNeasy mini kit (Qiagen). Libraries were prepared with Qiagen miRNA library prep kit (Qiagen) and a 75-bp single-end sequencing was performed on a NextSeq500 (Illumina) at the UAB Genomics Core. Raw miRNA-Seq FASTQ reads were uploaded to Qiagen's GeneGlobe Data Analysis Center (https://geneglobe.qiagen.com/us/analyze/) for analysis. Briefly, the reads were trimmed, unique molecular identifier (UMI) sequences identified, and then aligned to miRbase (ver21)[76] and the mouse mm10 genome. This created a tab-delimited file containing the count reads and UMIs assigned to each miRNA. The UMIs were then normalized, and differential expression was calculated using DESeq2. For miRNA over-representation analysis, we curated the previous publications (at least 2 publications for one mouse model) and established the altered miRNA lists from several mouse models with sociability impairment[77-101]. The lists of miRNAs were converted to ver21 with miRBaseConverter[102]. Enrichment of altered miRNAs was analyzed with Fisher's exact test. P values from multiple testing were adjusted (q-value) using the Benjamini-Hochberg false discovery rate (FDR) with a significant level of 0.05. For pathway analysis of potential target genes of miRNAs, target genes of miRNAs were obtained with miRTarBase and TargetScan 8.0 [103, 104]. GO enrichment analysis of miRNA target genes was performed using Metascape as described above.

Brain slice electrophysiology

Adult mice were anesthetized through isoflurane inhalation and then decapitated. The brain was quickly removed and coronal mPFC slices of 300 μm were obtained using a Leica VT1200S

vibratome. The dissection buffer used for the slicing was at pH 7.3 and 305 mOsm, containing the following (in mM): 206 sucrose, 25 $NaHCO_3$, 2.5 KCl, 10 $MgSO_4$, 1.45 NaH_2PO_4, 0.5 $CaCl_2$, and 11 d-glucose). This buffer was kept oxygenated (5% CO_2–95% O_2) during the whole dissection. Slices were then transferred to a holding chamber containing artificial cerebrospinal fluid solution (aCSF), composed of the following (in mM): 126 NaCl, 26 $NaHCO_3$, 2.5 KCl, 1.45 NaH_2PO_4, 1 $MgCl_2$, 2 $CaCl_2$, and 9 d-glucose. Slices were kept oxygenated at room temperature (22–25 °C) for at least 1 h. After this resting period, they were transferred to a submersion-type recording chamber upon a modified microscope stage, and kept constantly perfused with oxygenated aCSF throughout the experiments. The temperature in the recording chamber was kept at 30 ± 1.5 ^{o}C using an inline heater (Warner Instruments). Recording electrodes pipettes were fabricated from borosilicate glass with input resistances of ~4–7 MΩ. We used a visualized slice setup under a differential interference contrast-equipped microscope to perform our electrophysiology experiments. Whole-cell patch-clamp recordings were made in neurons visually located in layers 2/3 and 5 of the prelimbic region of the mPFC. Spontaneous postsynaptic currents were recorded in voltage-clamp mode by using the SutterPatch double IPA system and SutterPatch software. We applied holding at -70 mV, and compensated the electrode and cell capacitance. For all experiments, recordings were taken only 5 minutes after the whole-cell configuration was achieved, to allow cell adaptation. Currents were recorded for 5 minutes for all experiments. We included in our data only recordings from cells in which the access resistance did not change more than 20% during the recording and that displayed relatively stable baselines. Synaptic currents were detected and measured using SutterPatch software in-built system for analysis, and average amplitude e frequency of events for each cell was taken for statistical analysis. For sEPSC experiments, the $GABA_A$ antagonist bicuculline at 20 μM plus the NMDA antagonist D-APV at 50 μM were added to the bath, to isolate AMPA currents. The intracellular solution used was K^+ based and contained the following (in mM): 117 K-gluconate, 10 HEPES, 2 Na_2ATP, 0.4 Na_2GTP, 1 $MgCl_2$, 0.1 EGTA, 13 KCl, 0.07 $CaCl_2$, at pH

7.3, and 290 mOsm. For sIPSC experiments, the AMPA antagonist DNQX at 20 μM plus the NMDA antagonist D-APV at 50 μM were added to the bath, to isolate GABAergic currents. The intracellular solution used was Cs based and contained the following (in mM): 140 CsCl, 10 HEPES, 2 Na_2ATP, 0.4 Na_2GTP, 1 $MgCl_2$, 0.05 EGTA, 3.6 NaCl, at pH 7.3, and 290 mOsm. For the experiments where EVs were used, we added the EVs directly to the bath at a concentration of 2 x 10^7, and allowed the slices to incubate for at least one hour before starting the experiments. Recordings were taken while constantly perfused by this aCSF with the EVs added.

RNase and detergent treatment of EVs

EVs were mixed with or without 1 μl RNaseA (ThermoFisfer, EN0531) and 10 μl Triton X-100 (Sigma, T2199) and adjusted up to 200 μl by PBS. All samples were then incubated at 37 °C for 30 min, followed by heat inactivation of RNase at 95 °C for 10 min. After samples had cooled, RNA was extracted using miRNEasy mini kit (Qiagen) according to the manufacturer's protocol.

Quantitative reverse-transcription PCR (qRT-PCR) of miRNAs

EV-derived RNA (30 ng) was used to synthesize cDNA using miRCURY LNA RT kit (Qiagen). The cDNAs were then diluted at 1:30 and qPCR was performed using 2x miRCURY SYBR Green master mix (Qiagen) and miRCURY LNA miRNA PCR Assays (#339306, YP00204772 for miR-23a-3p and #339306, YP00204063 for miR-103-3p, Qiagen) with 95 °C for 2 min, 50 cycles of 95 °C for 10 s, and 56 °C for 60 s, on a C1000 Touch Thermal Cycler with CFX96 Real Time PCR Detection System (Bio-Rad). Cycle threshold (Ct) values were averaged across triplicates per experiment and per target. ΔCt was calculated to compare the data between groups.

EV small RNA extraction and supplementation to other EVs

Small RNAs were extracted from EVs using miRNEasy mini kit (#217004, Qiagen). The extracted RNAs (25 ng) were mixed with 2 x 10^9 EV particles using Exo-Fect Exosome transfection kit. EVs loaded with small RNAs were then reconstituted with 100 µl of DMEM media and transferred intravenously into recipient mice via retro-orbital injection.

EV loading with miR-23a-3p and miR-103a-3p mimics

miRNA mimic of 23a-3p (250 pmol, #339173 YM00470983-ADA, Qiagen) and 103a-3p (250 pmol, ##339173 YM 00470828-ADA, Qiagen) or negative control (500 pmol, #339173 YM00479902-ADA, Qiagen) were mixed with 2 x 10^9 EV particles using Exo-Fect Exosome transfection kit (#EXFT20A-1, System Biosciences) according to the manufacturer's instruction. EVs containing miRNAs or negative controls were re-constituted with 100 µl of Dulbecco's Modified Eagle Medium (#11965-092, Gibco) and then injected intravenously into recipient mice.

Statistical analysis

Normality and homogeneity of variances were initially assessed for all data sets. Data were analyzed with unpaired Student's *t* test, and one-way ANOVA, using GraphPad Prism 7 (GraphPad Software), SPSS and R. Other analyses such as Kruskal-Wallis and Linear Regression were used when appropriate. *Post hoc* analyses were performed using Dunnett's (one-way ANOVA), Dunn's (for Kruskal-Wallis), Games-Howell's (for Welch ANOVA), or Bonferroni adjustments. $p < 0.05$ was considered statistically significant and adjusted for multiple comparisons. All data is reported as mean ± standard error of the mean. Supplementary Table 13 provides the details of each analysis, including F values, sample sizes and size effects.

Data Availability

Raw RNA sequencing data will be available from NCBI Gene Expression Omnibus (GEO) database upon publication.

Code Availability

All analyses have been carried out using freely available software packages cited in the Methods section.

References

1. Villeda, S.A.*, et al.* Young blood reverses age-related impairments in cognitive function and synaptic plasticity in mice. *Nat Med* **20**, 659-663 (2014).
2. Castellano, J.M.*, et al.* Human umbilical cord plasma proteins revitalize hippocampal function in aged mice. *Nature* **544**, 488-492 (2017).
3. Cushman, J., Lo, J., Huang, Z., Wasserfall, C. & Petitto, J.M. Neurobehavioral changes resulting from recombinase activation gene 1 deletion. *Clinical and diagnostic laboratory immunology* **10**, 13-18 (2003).
4. Derecki, N.C.*, et al.* Regulation of learning and memory by meningeal immunity: a key role for IL-4. *J Exp Med* **207**, 1067-1080 (2010).
5. Filiano, A.J.*, et al.* Unexpected role of interferon-gamma in regulating neuronal connectivity and social behaviour. *Nature* **535**, 425-429 (2016).
6. Smith, C.J.*, et al.* Probiotics normalize the gut-brain-microbiota axis in immunodeficient mice. *Am J Physiol Gastrointest Liver Physiol* **307**, G793-802 (2014).
7. Reed, M.D.*, et al.* IL-17a promotes sociability in mouse models of neurodevelopmental disorders. *Nature* **577**, 249-253 (2020).
8. Kawamoto, S.*, et al.* Foxp3(+) T cells regulate immunoglobulin a selection and facilitate diversification of bacterial species responsible for immune homeostasis. *Immunity* **41**, 152-165 (2014).
9. Miyajima, M.*, et al.* Metabolic shift induced by systemic activation of T cells in PD-1-deficient mice perturbs brain monoamines and emotional behavior. *Nat Immunol* **18**, 1342-1352 (2017).
10. de Candia, P.*, et al.* The circulating microRNome demonstrates distinct lymphocyte subset-dependent signatures. *Eur J Immunol* **46**, 725-731 (2016).

11. Clark, S.M., Vaughn, C.N., Soroka, J.A., Li, X. & Tonelli, L.H. Neonatal adoptive transfer of lymphocytes rescues social behaviour during adolescence in immune-deficient mice. *Eur J Neurosci* **47**, 968-978 (2018).

12. Yanez-Mo, M.*, et al.* Biological properties of extracellular vesicles and their physiological functions. *J Extracell Vesicles* **4**, 27066 (2015).

13. van Niel, G., D'Angelo, G. & Raposo, G. Shedding light on the cell biology of extracellular vesicles. *Nat Rev Mol Cell Biol* **19**, 213-228 (2018).

14. Kano, S.I., Dohi, E. & Rose, I.V.L. Extracellular Vesicles for Research on Psychiatric Disorders. *Schizophr Bull* **45**, 7-16 (2019).

15. Valadi, H.*, et al.* Exosome-mediated transfer of mRNAs and microRNAs is a novel mechanism of genetic exchange between cells. *Nat Cell Biol* **9**, 654-659 (2007).

16. Gross, J.C., Chaudhary, V., Bartscherer, K. & Boutros, M. Active Wnt proteins are secreted on exosomes. *Nat Cell Biol* **14**, 1036-1045 (2012).

17. O'Brien, K., Breyne, K., Ughetto, S., Laurent, L.C. & Breakefield, X.O. RNA delivery by extracellular vesicles in mammalian cells and its applications. *Nat Rev Mol Cell Biol* **21**, 585-606 (2020).

18. Thomou, T.*, et al.* Adipose-derived circulating miRNAs regulate gene expression in other tissues. *Nature* **542**, 450-455 (2017).

19. Zhao, Y.*, et al.* Liver governs adipose remodelling via extracellular vesicles in response to lipid overload. *Nat Commun* **11**, 719 (2020).

20. Lee, Y.*, et al.* Rapid Assessment of Microbiota Changes in Individuals with Autism Spectrum Disorder Using Bacteria-derived Membrane Vesicles in Urine. *Exp Neurobiol* **26**, 307-317 (2017).

21. Tsilioni, I. & Theoharides, T.C. Extracellular vesicles are increased in the serum of children with autism spectrum disorder, contain mitochondrial DNA, and stimulate human microglia to secrete IL-1beta. *J Neuroinflammation* **15**, 239 (2018).

22. Qin, Y.*, et al.* Whole-Transcriptome Analysis of Serum L1CAM-Captured Extracellular Vesicles Reveals Neural and Glycosylation Changes in Autism Spectrum Disorder. *J Mol Neurosci* **72**, 1274-1292 (2022).

23. Du, Y.*, et al.* Metabolomic Identification of Exosome-Derived Biomarkers for Schizophrenia: A Large Multicenter Study. *Schizophr Bull* **47**, 615-623 (2021).

24. Du, Y.*, et al.* Genome-Wide, Integrative Analysis Implicates Exosome-Derived MicroRNA Dysregulation in Schizophrenia. *Schizophr Bull* **45**, 1257-1266 (2019).

25. Kapogiannis, D.*, et al.* Association of Extracellular Vesicle Biomarkers With Alzheimer Disease in the Baltimore Longitudinal Study of Aging. *JAMA Neurol* **76**, 1340-1351 (2019).

26. Li, T.R.*, et al.* beta-Amyloid in blood neuronal-derived extracellular vesicles is elevated in cognitively normal adults at risk of Alzheimer's disease and predicts cerebral amyloidosis. *Alzheimers Res Ther* **14**, 66 (2022).

27. Honorato-Mauer, J.*, et al.* Alterations in microRNA of extracellular vesicles associated with major depression, attention-deficit/hyperactivity and anxiety disorders in adolescents. *Transl Psychiatry* **13**, 47 (2023).

28. Xie, X.H.*, et al.* Hyper-inflammation of astrocytes in patients of major depressive disorder: Evidence from serum astrocyte-derived extracellular vesicles. *Brain Behav Immun* **109**, 51-62 (2023).

29. Osborne, L.M., Payne, J.L., Sherer, M.L. & Sabunciyan, S. Altered extracellular mRNA communication in postpartum depression is associated with decreased autophagy. *Mol Psychiatry* **27**, 4526-4535 (2022).

30. Goetzl, E.J.*, et al.* Abnormal levels of mitochondrial proteins in plasma neuronal extracellular vesicles in major depressive disorder. *Mol Psychiatry* **26**, 7355-7362 (2021).

31. Nasca, C.*, et al.* Insulin receptor substrate in brain-enriched exosomes in subjects with major depression: on the path of creation of biosignatures of central insulin resistance. *Mol Psychiatry* **26**, 5140-5149 (2021).

32. Wei, Z.X.*, et al.* Exosomes from patients with major depression cause depressive-like behaviors in mice with involvement of miR-139-5p-regulated neurogenesis. *Neuropsychopharmacology* **45**, 1050-1058 (2020).

33. Wang, J.*, et al.* Extracellular vesicles mediate the communication of adipose tissue with brain and promote cognitive impairment associated with insulin resistance. *Cell Metab* **34**, 1264-1279 e1268 (2022).

34. Verweij, F.J.*, et al.* The power of imaging to understand extracellular vesicle biology in vivo. *Nat Methods* **18**, 1013-1026 (2021).

35. Muzumdar, M.D., Tasic, B., Miyamichi, K., Li, L. & Luo, L. A global double-fluorescent Cre reporter mouse. *Genesis* **45**, 593-605 (2007).

36. Yizhar, O.*, et al.* Neocortical excitation/inhibition balance in information processing and social dysfunction. *Nature* **477**, 171-178 (2011).

37. Bicks, L.K., Koike, H., Akbarian, S. & Morishita, H. Prefrontal Cortex and Social Cognition in Mouse and Man. *Front Psychol* **6**, 1805 (2015).

38. Chen, P. & Hong, W. Neural Circuit Mechanisms of Social Behavior. *Neuron* **98**, 16-30 (2018).

39. Yizhar, O. & Levy, D.R. The social dilemma: prefrontal control of mammalian sociability. *Curr Opin Neurobiol* **68**, 67-75 (2021).

40. Roth, B.L. DREADDs for Neuroscientists. *Neuron* **89**, 683-694 (2016).

41. Castano, C., Mirasierra, M., Vallejo, M., Novials, A. & Parrizas, M. Delivery of muscle-derived exosomal miRNAs induced by HIIT improves insulin sensitivity through down-regulation of hepatic FoxO1 in mice. *Proceedings of the National Academy of Sciences of the United States of America* **117**, 30335-30343 (2020).

42. Chou, W.H.*, et al.* GABAA receptor trafficking is regulated by protein kinase C(epsilon) and the N-ethylmaleimide-sensitive factor. *J Neurosci* **30**, 13955-13965 (2010).

43. Shurtleff, M.J., Temoche-Diaz, M.M., Karfilis, K.V., Ri, S. & Schekman, R. Y-box protein 1 is required to sort microRNAs into exosomes in cells and in a cell-free reaction. *Elife* **5** (2016).

44. Barman, B.*, et al.* VAP-A and its binding partner CERT drive biogenesis of RNA-containing extracellular vesicles at ER membrane contact sites. *Dev Cell* **57**, 974-994 e978 (2022).

45. Kurkewich, J.L.*, et al.* The mirn23a microRNA cluster antagonizes B cell development. *J Leukoc Biol* **100**, 665-677 (2016).

46. Rajgor, D.*, et al.* Local miRNA-Dependent Translational Control of GABA(A)R Synthesis during Inhibitory Long-Term Potentiation. *Cell Rep* **31**, 107785 (2020).

47. Osten, P., Valsamis, L., Harris, A. & Sacktor, T.C. Protein synthesis-dependent formation of protein kinase Mzeta in long-term potentiation. *J Neurosci* **16**, 2444-2451 (1996).

48. Glock, C.*, et al.* The translatome of neuronal cell bodies, dendrites, and axons. *Proc Natl Acad Sci U S A* **118** (2021).

49. Herz, J.*, et al.* GABAergic neuronal IL-4R mediates T cell effect on memory. *Neuron* **109**, 3609-3618 e3609 (2021).

50. Mittelbrunn, M.*, et al.* Unidirectional transfer of microRNA-loaded exosomes from T cells to antigen-presenting cells. *Nat Commun* **2**, 282 (2011).

51. Okoye, I.S.*, et al.* MicroRNA-containing T-regulatory-cell-derived exosomes suppress pathogenic T helper 1 cells. *Immunity* **41**, 89-103 (2014).

52. Verweij, F.J.*, et al.* Live Tracking of Inter-organ Communication by Endogenous Exosomes In Vivo. *Dev Cell* **48**, 573-589 e574 (2019).

53. Ferris, E.*, et al.* Genomic convergence in hibernating mammals elucidates the genetics of metabolic regulation in the hypothalamus. *Science* **389**, 494-500 (2025).

54. Wu, Y.E., Parikshak, N.N., Belgard, T.G. & Geschwind, D.H. Genome-wide, integrative analysis implicates microRNA dysregulation in autism spectrum disorder. *Nat Neurosci* **19**, 1463-1476 (2016).

55. Jin, M.*, et al.* Establishment of a schizophrenia classifier based on peripheral blood signatures and investigation of pathogenic miRNA-mRNA regulation. *J Psychiatr Res* **159**, 172-184 (2023).

56. Jyonouchi, H.*, et al.* Serum microRNAs in ASD: Association With Monocyte Cytokine Profiles and Mitochondrial Respiration. *Front Psychiatry* **10**, 614 (2019).

57. Huang, F.*, et al.* Investigation of Gene Regulatory Networks Associated with Autism Spectrum Disorder Based on MiRNA Expression in China. *PLoS One* **10**, e0129052 (2015).

58. Vassileff, N., Cheng, L. & Hill, A.F. Extracellular vesicles - propagators of neuropathology and sources of potential biomarkers and therapeutics for neurodegenerative diseases. *J Cell Sci* **133** (2020).

59. Moy, S.S.*, et al.* Sociability and preference for social novelty in five inbred strains: an approach to assess autistic-like behavior in mice. *Genes Brain Behav* **3**, 287-302 (2004).

60. Dohi, E.*, et al.* Behavioral Changes in Mice Lacking Interleukin-33. *eNeuro* **4** (2017).

61. Yang, M. & Crawley, J.N. Simple behavioral assessment of mouse olfaction. *Curr Protoc Neurosci* **Chapter 8**, Unit 8 24 (2009).

62. Niwa, M.*, et al.* Knockdown of DISC1 by in utero gene transfer disturbs postnatal dopaminergic maturation in the frontal cortex and leads to adult behavioral deficits. *Neuron* **65**, 480-489 (2010).

63. Thery, C.*, et al.* Minimal information for studies of extracellular vesicles 2018 (MISEV2018): a position statement of the International Society for Extracellular Vesicles and update of the MISEV2014 guidelines. *J Extracell Vesicles* **7**, 1535750 (2018).

64. Sakamoto, S.*, et al.* Alterations in circulating extracellular vesicles underlie social stress-induced behaviors in mice. *FEBS Open Bio* **11**, 2678-2692 (2021).

65. Arab, T.*, et al.* Characterization of extracellular vesicles and synthetic nanoparticles with four orthogonal single-particle analysis platforms. *J Extracell Vesicles* **10**, e12079 (2021).

66. Kano, S.*, et al.* The contribution of transcription factor IRF1 to the interferon-gamma-interleukin 12 signaling axis and TH1 versus TH-17 differentiation of CD4+ T cells. *Nat Immunol* **9**, 34-41 (2008).

67. Klein, H. & Anstee, D. *Mollison's Blood Transfusion in Clinical Medicine* (2005).

68. Boulton, F. The 13% rule. in *Transfusion Today* 7-9 (International Society of Blood Transfusion, 2007).

69. Bariselli, S.*, et al.* Role of VTA dopamine neurons and neuroligin 3 in sociability traits related to nonfamiliar conspecific interaction. *Nat Commun* **9**, 3173 (2018).

70. Kano, S.I.*, et al.* Glutathione S-transferases promote proinflammatory astrocyte-microglia communication during brain inflammation. *Sci Signal* **12** (2019).

71. Schindelin, J.*, et al.* Fiji: an open-source platform for biological-image analysis. *Nat Methods* **9**, 676-682 (2012).

72. Dobin, A.*, et al.* STAR: ultrafast universal RNA-seq aligner. *Bioinformatics* **29**, 15-21 (2013).

73. Anders, S., Pyl, P.T. & Huber, W. HTSeq--a Python framework to work with high-throughput sequencing data. *Bioinformatics* **31**, 166-169 (2015).

74. Love, M.I., Huber, W. & Anders, S. Moderated estimation of fold change and dispersion for RNA-seq data with DESeq2. *Genome Biol* **15**, 550 (2014).

75. Zhou, Y.*, et al.* Metascape provides a biologist-oriented resource for the analysis of systems-level datasets. *Nat Commun* **10**, 1523 (2019).

76. Kozomara, A. & Griffiths-Jones, S. miRBase: annotating high confidence microRNAs using deep sequencing data. *Nucleic Acids Res* **42**, D68-73 (2014).

77. Urdinguio, R.G.*, et al.* Disrupted microRNA expression caused by Mecp2 loss in a mouse model of Rett syndrome. *Epigenetics* **5**, 656-663 (2010).

78. Wu, H.*, et al.* Genome-wide analysis reveals methyl-CpG-binding protein 2-dependent regulation of microRNAs in a mouse model of Rett syndrome. *Proc Natl Acad Sci U S A* **107**, 18161-18166 (2010).

79. Cheng, T.L.*, et al.* MeCP2 suppresses nuclear microRNA processing and dendritic growth by regulating the DGCR8/Drosha complex. *Dev Cell* **28**, 547-560 (2014).

80. Gao, Y.*, et al.* Inhibition of miR-15a Promotes BDNF Expression and Rescues Dendritic Maturation Deficits in MeCP2-Deficient Neurons. *Stem Cells* **33**, 1618-1629 (2015).

81. Edbauer, D.*, et al.* Regulation of synaptic structure and function by FMRP-associated microRNAs miR-125b and miR-132. *Neuron* **65**, 373-384 (2010).

82. Xu, X.L.*, et al.* FXR1P but not FMRP regulates the levels of mammalian brain-specific microRNA-9 and microRNA-124. *J Neurosci* **31**, 13705-13709 (2011).

83. Liu, T.*, et al.* A MicroRNA Profile in Fmr1 Knockout Mice Reveals MicroRNA Expression Alterations with Possible Roles in Fragile X Syndrome. *Mol Neurobiol* **51**, 1053-1063 (2015).

84. Zhang, M.*, et al.* Identification of differentially expressed microRNAs and their target genes in the hippocampal tissues of Fmr1 knockout mice. *Am J Transl Res* **12**, 813-824 (2020).

85. Hara, Y.*, et al.* Prenatal exposure to valproic acid increases miR-132 levels in the mouse embryonic brain. *Mol Autism* **8**, 33 (2017).

86. Ozkul, Y.*, et al.* A heritable profile of six miRNAs in autistic patients and mouse models. *Sci Rep* **10**, 9011 (2020).

87. Kumari, A., Singh, P., Baghel, M.S. & Thakur, M.K. Social isolation mediated anxiety like behavior is associated with enhanced expression and regulation of BDNF in the female mouse brain. *Physiol Behav* **158**, 34-42 (2016).

88. Chang, C.H., Kuek, E.J.W., Su, C.L. & Gean, P.W. MicroRNA-206 Regulates Stress-Provoked Aggressive Behaviors in Post-weaning Social Isolation Mice. *Mol Ther Nucleic Acids* **20**, 812-822 (2020).

89. Popa, N., Boyer, F., Jaouen, F., Belzeaux, R. & Gascon, E. Social Isolation and Enrichment Induce Unique miRNA Signatures in the Prefrontal Cortex and Behavioral Changes in Mice. *iScience* **23**, 101790 (2020).

90. Haramati, S.*, et al.* MicroRNA as repressors of stress-induced anxiety: the case of amygdalar miR-34. *J Neurosci* **31**, 14191-14203 (2011).

91. Dias, C.*, et al.* beta-catenin mediates stress resilience through Dicer1/microRNA regulation. *Nature* **516**, 51-55 (2014).

92. Torres-Berrio, A.*, et al.* DCC Confers Susceptibility to Depression-like Behaviors in Humans and Mice and Is Regulated by miR-218. *Biol Psychiatry* **81**, 306-315 (2017).

93. Volk, N.*, et al.* Amygdalar MicroRNA-15a Is Essential for Coping with Chronic Stress. *Cell Rep* **17**, 1882-1891 (2016).

94. Deng, Z.F.*, et al.* miR-214-3p Targets beta-Catenin to Regulate Depressive-like Behaviors Induced by Chronic Social Defeat Stress in Mice. *Cereb Cortex* **29**, 1509-1519 (2019).

95. Du, K., Lu, W., Sun, Y., Feng, J. & Wang, J.H. mRNA and miRNA profiles in the nucleus accumbens are related to fear memory and anxiety induced by physical or psychological stress. *J Psychiatr Res* **118**, 44-65 (2019).

96. Khandelwal, N., Dey, S.K., Chakravarty, S. & Kumar, A. miR-30 Family miRNAs Mediate the Effect of Chronic Social Defeat Stress on Hippocampal Neurogenesis in Mouse Depression Model. *Front Mol Neurosci* **12**, 188 (2019).

97. Torres-Berrio, A.*, et al.* miR-218 in Adolescence Predicts and Mediates Vulnerability to Stress. *Biol Psychiatry* **89**, 911-919 (2021).

98. Miao, Z.*, et al.* Presence of the pregnant partner regulates microRNA-30a and BDNF levels and protects male mice from social defeat-induced abnormal behaviors. *Neuropharmacology* **159**, 107589 (2019).

99. Pfau, M.L.*, et al.* Role of Monocyte-Derived MicroRNA106b approximately 25 in Resilience to Social Stress. *Biol Psychiatry* **86**, 474-482 (2019).

100. Luo, P.X.*, et al.* Sex-specific effects of social defeat stress on miRNA expression in the anterior BNST. *Behav Brain Res* **401**, 113084 (2021).

101. Miao, Z.*, et al.* Anxiety-Related Behaviours Associated with microRNA-206-3p and BDNF Expression in Pregnant Female Mice Following Psychological Social Stress. *Mol Neurobiol* **55**, 1097-1111 (2018).

102. Xu, T.*, et al.* miRBaseConverter: an R/Bioconductor package for converting and retrieving miRNA name, accession, sequence and family information in different versions of miRBase. *BMC Bioinformatics* **19**, 514 (2018).

103. Huang, H.Y.*, et al.* miRTarBase 2020: updates to the experimentally validated microRNA-target interaction database. *Nucleic Acids Res* **48**, D148-D154 (2020).

104. Santovito, D.*, et al.* Plasma microRNA signature associated with retinopathy in patients with type 2 diabetes. *Sci Rep* **11**, 4136 (2021).

Acknowledgements

We thank J. Kang, D. Mallah, D. Medeiros, B. Lo, S. Gonzalez, T. Wan, S. Kou, A. Murata, Y. Kobayashi, E. Mallick, D. Muth, D. Wilson, J. Green, H. Morishita, and T. Akimoto for technical help and advice; R. Dahl for *Mir23a*$^{-/-}$ mice. We also thank the UAB Animal Behavioral Assessment core, the UAB Civitan International Research Center, the UAB Genomics core, the UAB High Resolution Imaging Facility core, the UAB Center for Neurodegeneration and Experimental Therapeutics, and the JHU School of Medicine Microscope Facility for shared resources. This work was made possible by support from the Johns Hopkins Medicine Discovery Fund (to S-i.K.) and the National Institutes of Health (MH093458, MH113645, and MH118492 to S-i.K.). K.W.W. and S-i.K. are supported by Allen Distinguished Investigator awards through the Paul G. Allen Frontiers Group.

Author Contributions

S-i.K. initially conceived the project with E.D. K.M., E.D., P.A.G., J.F-O., M.M., I.B., F.A., J.B., O.F., E.Y.C., J.S., T.K., N.I., R.M., I.V.L.R., and T.I. conducted the experiments and analyzed the data. D.K.C., E.D., and S-i.K. performed RNA-seq and miRNA-seq data analyses. M.V.P., K.W.W., and M.N. provided their respective expertise related to behavioral assays, extracellular vesicle analysis, and *in vivo* neuronal manipulation. S-i.K. wrote the original draft manuscript with E.D., K.M., J.F-O., and P.A.G., and edited it with the inputs from co-authors.

Competing Interests

S-i. K. is an inventor on a patent application related to the work published in this paper.

Fig. 1

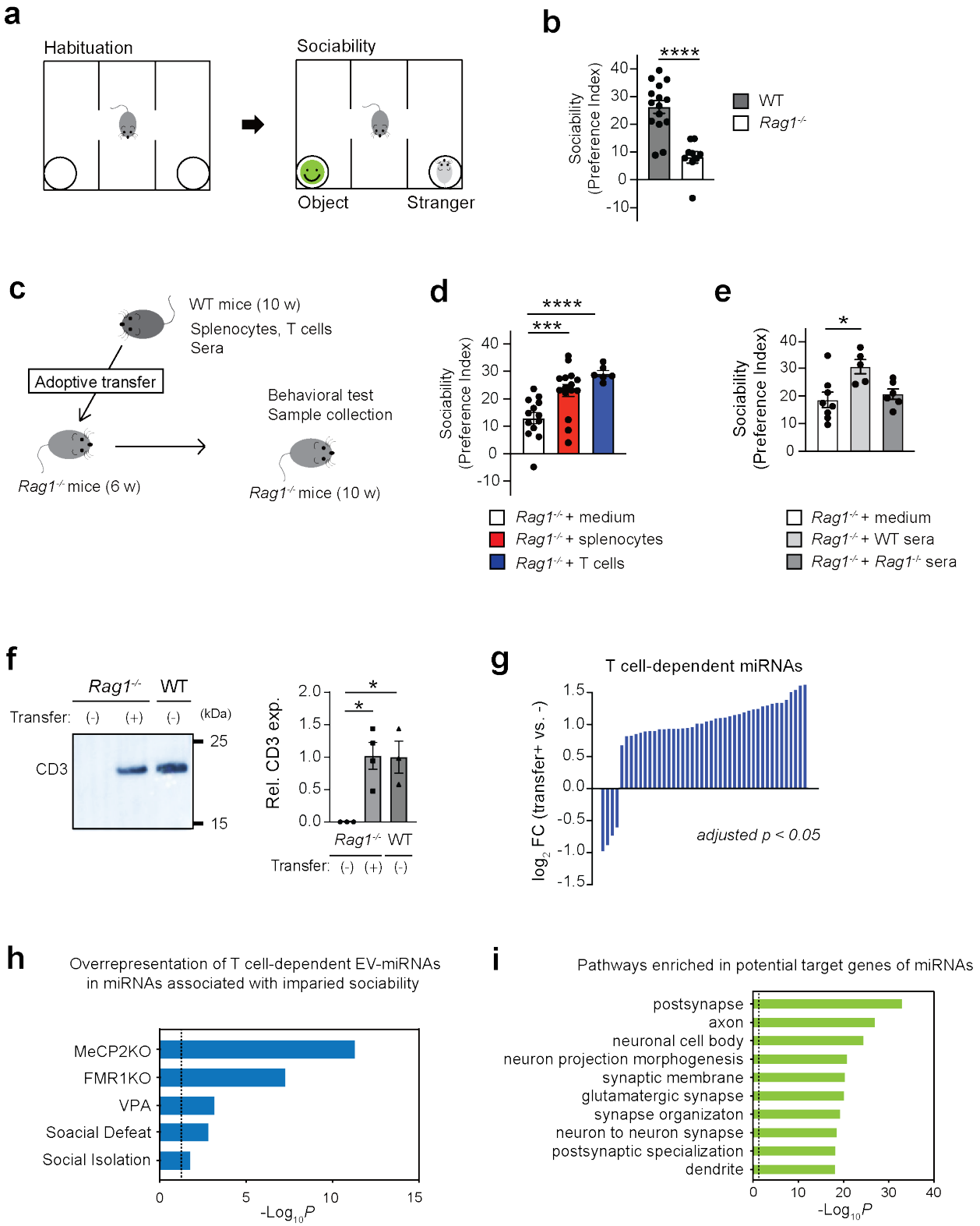
a
Habituation
Sociability
Object
Stranger
b
****
Sociability (Preference Index)
40
30
20
10
0
-10
WT
Rag1-/-
c
WT mice (10 w)
Splenocytes, T cells
Sera
Adoptive transfer
Behavioral test
Sample collection
Rag1-/- mice (6 w)
Rag1-/- mice (10 w)
d
****
***
Sociability (Preference Index)
Rag1-/- + medium
Rag1-/- + splenocytes
Rag1-/- + T cells
e
*
Sociability (Preference Index)
Rag1-/- + medium
Rag1-/- + WT sera
Rag1-/- + Rag1-/- sera
f
Rag1-/-
WT
Transfer: (-) (+) (-)
(kDa)
CD3
25
15
Rel. CD3 exp.
2.0
1.5
1.0
0.5
0.0
*
*
Rag1-/- WT
Transfer: (-) (+) (-)
g
T cell-dependent miRNAs
log2 FC (transfer+ vs. -)
1.5
1.0
0.5
0.0
-0.5
-1.0
-1.5
adjusted p < 0.05
h
Overrepresentation of T cell-dependent EV-miRNAs
in miRNAs associated with imparied sociability
MeCP2KO
FMR1KO
VPA
Soacial Defeat
Social Isolation
0
5
10
15
-Log10P
i
Pathways enriched in potential target genes of miRNAs
postsynapse
axon
neuronal cell body
neuron projection morphogenesis
synaptic membrane
glutamatergic synapse
synapse organizaton
neuron to neuron synapse
postsynaptic specialization
dendrite
0
10
20
30
40
-Log10P

Figure. 1: Serum injection as well as T cell transfer from WT mice improves sociability in *Rag1*$^{-/-}$ mice. a, Outline of the three-chamber sociability test. **b**, Sociability in the three-chamber social interaction test by WT and *Rag1*$^{-/-}$ mice. WT mice, n = 15; *Rag1*$^{-/-}$ mice, n = 9. **c**, Experimental outline of adoptive transfer/serum injection and subsequent behavioral assay. **d**, Adoptive transfer of WT mouse splenocytes or T cells into *Rag1*$^{-/-}$ mice increased their sociability. *Rag1*$^{-/-}$ mice + medium, n = 13; *Rag1*$^{-/-}$ mice + WT splenocytes, n = 15; and *Rag1*$^{-/-}$ mice + WT T cells, n = 6. **e**, Intravenous injection of sera from WT mice, but not from *Rag1*$^{-/-}$ mice, into *Rag1*$^{-/-}$ mice increased their sociability. *Rag1*$^{-/-}$ mice + medium, n = 8; *Rag1*$^{-/-}$ mice + WT sera, n = 5; and *Rag1*$^{-/-}$ mice + *Rag1*$^{-/-}$ sera, n = 6. **f,** Presence of CD3^{+} EVs in WT and *Rag1*$^{-/-}$ samples (n=3 per group). Left, representative Western blot images showing the recovery of CD3^{+} bEVs upon the adoptive transfer of WT mouse splenocytes into *Rag1*$^{-/-}$ mice. Right, quantification graphs. **g,** Waterfall plot representing the bEV miRNAs whose expression significantly changed (adjusted $p < 0.05$) by the adoptive transfer of WT T cells into *Rag1*$^{-/-}$ mice. These miRNAs are regarded as T cell-dependent EV-miRNAs. *Rag1*$^{-/-}$ mice, n = 6; *Rag1*$^{-/-}$ mice + WT T cells, n = 6**. h,** T cell-dependent EV miRNAs were over-represented by the miRNAs whose expression changes were previously observed in the mice with sociability deficits. The list of miRNAs were curated from the previous publications (at least 2 publications for each mouse model) on several mouse models with sociability impairment [77-101]. Enrichment was calculated with Fisher's exact test. **i,** Potential target genes of T cell-dependent EV miRNAs were enriched in the regulation of synapses and neurons. Each bar represent mean ± SEM. Each dot represents one mouse. ns, not significant. *p<0.05, ***p <0.005, ****p<0.001. Significance was determined by Student's *t* test and one-way ANOVA with *post hoc* Dunnett's test. See Supplementary Table 13 for the detail of statistical analysis.

Fig. 2

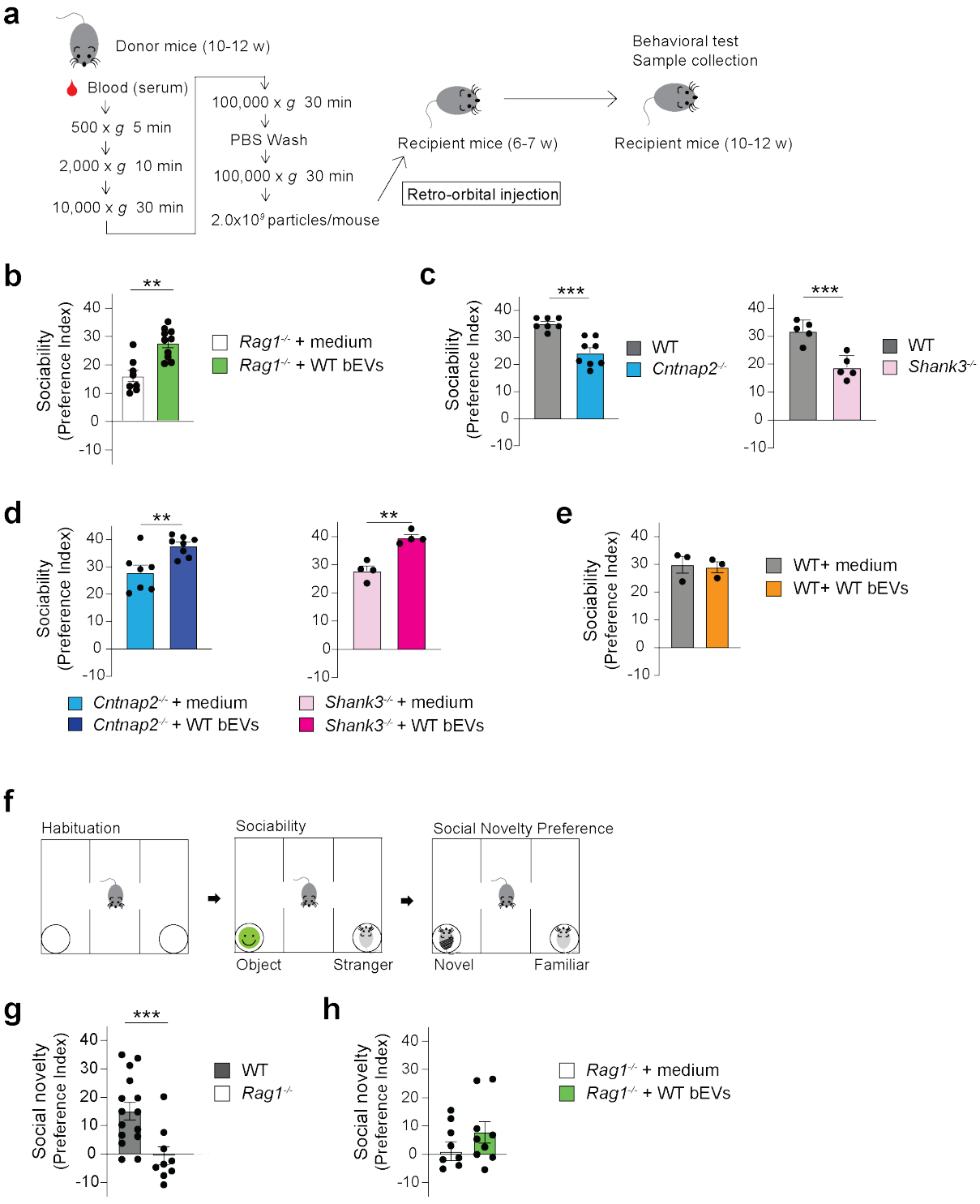
a
Donor mice (10-12 w)
Blood (serum)
500 x g 5 min
2,000 x g 10 min
10,000 x g 30 min
100,000 x g 30 min
PBS Wash
100,000 x g 30 min
2.0x10⁹ particles/mouse
Recipient mice (6-7 w)
Retro-orbital injection
Behavioral test
Sample collection
Recipient mice (10-12 w)
b
Sociability (Preference Index)
Rag1-/- + medium
Rag1-/- + WT bEVs
c
WT
Cntnap2-/-
Shank3-/-
d
Cntnap2-/- + medium
Cntnap2-/- + WT bEVs
Shank3-/- + medium
Shank3-/- + WT bEVs
e
WT+ medium
WT+ WT bEVs
f
Habituation
Sociability
Social Novelty Preference
Object
Stranger
Novel
Familiar
g
Social novelty (Preference Index)
WT
Rag1-/-
h

Fig. 2: WT bEVs improve sociability in *Rag1*$^{-/-}$ mice and two additional mouse models with sociability deficits. a, Experimental outline of bEV collection, intravenous injection, and subsequent behavioral assay. **b,** Intravenous injection of WT bEVs into *Rag1*$^{-/-}$ mice increased their sociability deficits. *Rag1*$^{-/-}$ mice + medium, n = 8; *Rag1*$^{-/-}$ mice + WT EVs, n = 10. **c,** *Cntnap2*$^{-/-}$ and *Shank3*$^{-/-}$ mice showed a reduced preference for interacting with the mouse versus the object (sociability deficits) in the three-chamber social interaction test. **d.** Intravenous injection of WT bEVs into *Cntnap2*$^{-/-}$ and *Shank3*$^{-/-}$ mice increased their sociability deficits. **e,** Intravenous injection of WT bEVs did not enhance sociability in WT mice. WT mice + medium, n = 3; and WT mice + WT bEVs, n = 3. **f,** Outline of the three-chamber social novelty recognition test. **g,** *Rag1*$^{-/-}$ mice also showed a reduced preference in interacting with a novel mouse versus a familiar mouse (social novel preference deficits) in the three-chamber social interaction test. WT mice, n = 15; and *Rag1*$^{-/-}$ mice, n = 9. **h,** Intravenous injection of neither WT bEVs increased social novelty preference in *Rag1*$^{-/-}$ mice. *Rag1*$^{-/-}$ mice + medium, n = 8; *Rag1*$^{-/-}$ mice + WT EVs, n = 9. Each bar represent mean ± SEM. Each dot represents one mouse. ns, not significant. $^{**}p<0.01$, $^{***}p<0.005$. Significance was determined by Student's *t* test. See Supplementary Table 13 for the detail of statistical analysis.

Fig. 3

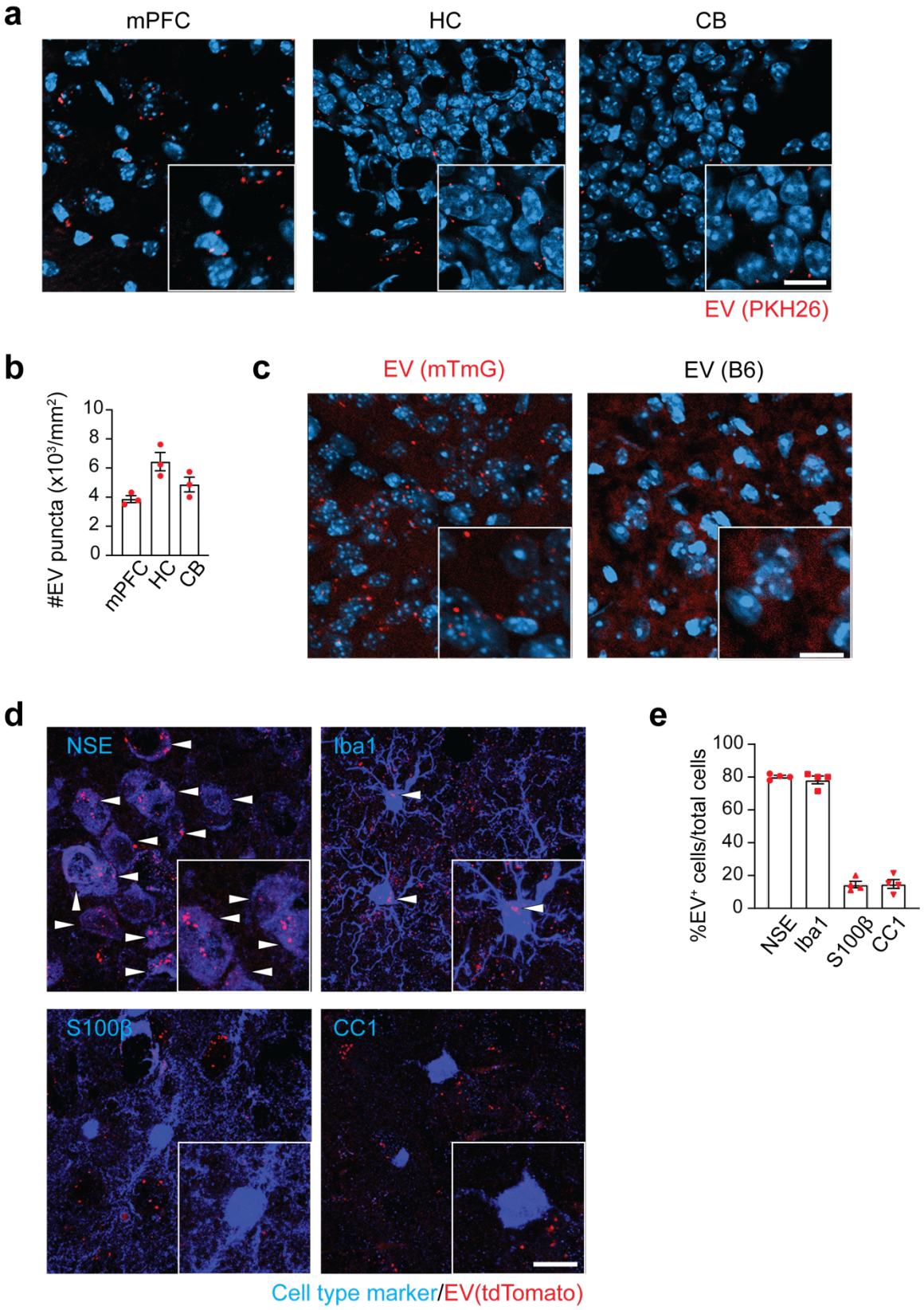
a
mPFC
HC
CB
EV (PKH26)
b
#EV puncta (x10³/mm²)
10
8
6
4
2
0
mPFC
HC
CB
c
EV (mTmG)
EV (B6)
d
NSE
Iba1
S100β
CC1
Cell type marker/EV(tdTomato)
e
%EV⁺ cells/total cells
100
80
60
40
20
0
NSE
Iba1
S100β
CC1

Fig. 3: Intravenously injected WT bEVs are co-localized to neurons and microglia in the brain parenchyma. a, Representative confocal microscope images showing the distribution patterns of intravenously injected PKH26-labeled EVs (Red) in the mPFC, hippocampus (HC) and cerebellum (CB) of *Rag1*$^{-/-}$ mice. DAPI stain (blue). **b,** Quantification of PKH26- labeled EVs in the brains of *Rag1*$^{-/-}$ mice (n = 3). **c,** Representative confocal microscope images showing the distribution patterns of intravenously injected tdTomato^{+} EVs (Red) from mTmG mice in the mPFC of *Rag1*$^{-/-}$ mice. DAPI stain (blue). **d** Representative confocal microscope images showing the localization of tdTomato^{+} EVs with neurons (NSE^{+} cells) and microglia (Iba1^{+} cells) in the mPFC of *Rag1*$^{-/-}$ mice. EV^{+} cells are indicated by white arrowheads. **e,** Quantification of tdTomato^{+} EVs localized with neurons (NSE^{+} cells), microglia (Iba1^{+} cells), astrocytes (S100β^{+} cells), and oligodendrocytes (CC1^{+} cells) in the mPFC of *Rag1*$^{-/-}$ mice (n = 4). Scale bar, 10 μm. Each bar represent mean ± SEM. Each dot represents one mouse.

Fig. 4

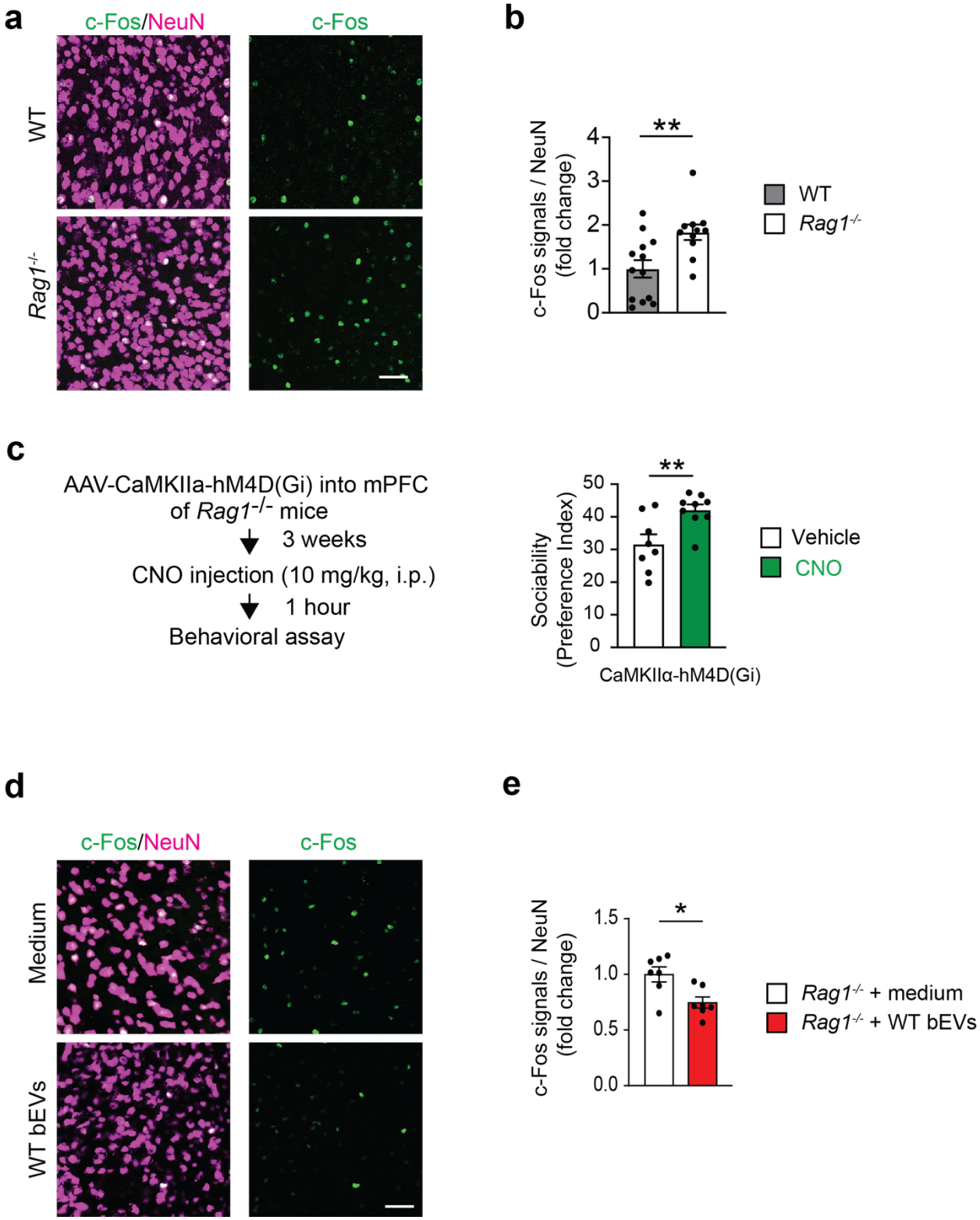
a
c-Fos/NeuN
c-Fos
WT
Rag1-/-
b
c-Fos signals / NeuN (fold change)
**
WT
Rag1-/-
c
AAV-CaMKIIa-hM4D(Gi) into mPFC of Rag1-/- mice
3 weeks
CNO injection (10 mg/kg, i.p.)
1 hour
Behavioral assay
Sociability (Preference Index)
**
Vehicle
CNO
CaMKIIα-hM4D(Gi)
d
c-Fos/NeuN
c-Fos
Medium
WT bEVs
e
c-Fos signals / NeuN (fold change)
*
Rag1-/- + medium
Rag1-/- + WT bEVs

Fig. 4: WT bEVs attenuate hyperexcitability in the mPFC of *Rag1*$^{-/-}$ mice. a, Representative confocal microscope images showing an enhanced c-Fos immunoreactivity in the mPFC of *Rag1*$^{-/-}$ mice. **b,** Quantification of c-Fos-positive neurons as fold change of percentages for c-Fos^{+} cells per NeuN^{+} cells. WT mice, n = 13 *Rag1*$^{-/-}$ mice, n = 11. **c,** Chemogenetic inhibition of CamKIIα^{+} neuronal activities in the mPFC by hM4D(Gi) upon CNO injection increased sociability in *Rag1*$^{-/-}$ mice. Vehicle n = 8 mice; CNO n = 9 mice. **d,** Representative confocal microscope images showed a reduction of c-Fos immunoreactivity in the mPFC of *Rag1*$^{-/-}$ mice after WT bEV injection. **e,** Quantification of c-Fos-positive neurons as fold-change of percentages for c-Fos^{+} cells per NeuN^{+} cells. *Rag1*$^{-/-}$ mice + medium, n = 7; *Rag1*$^{-/-}$ mice + WT EVs, n = 7. Scale bar, 50 μm. Each bar represent mean ± SEM. Each dot represents one mouse. ns, not significant. $^{**}p < 0.01$, $^{****}p < 0.001$. Significance was determined by Student's *t*-test. See Supplementary Table 13 for the detail of statistical analysis.

Fig. 5

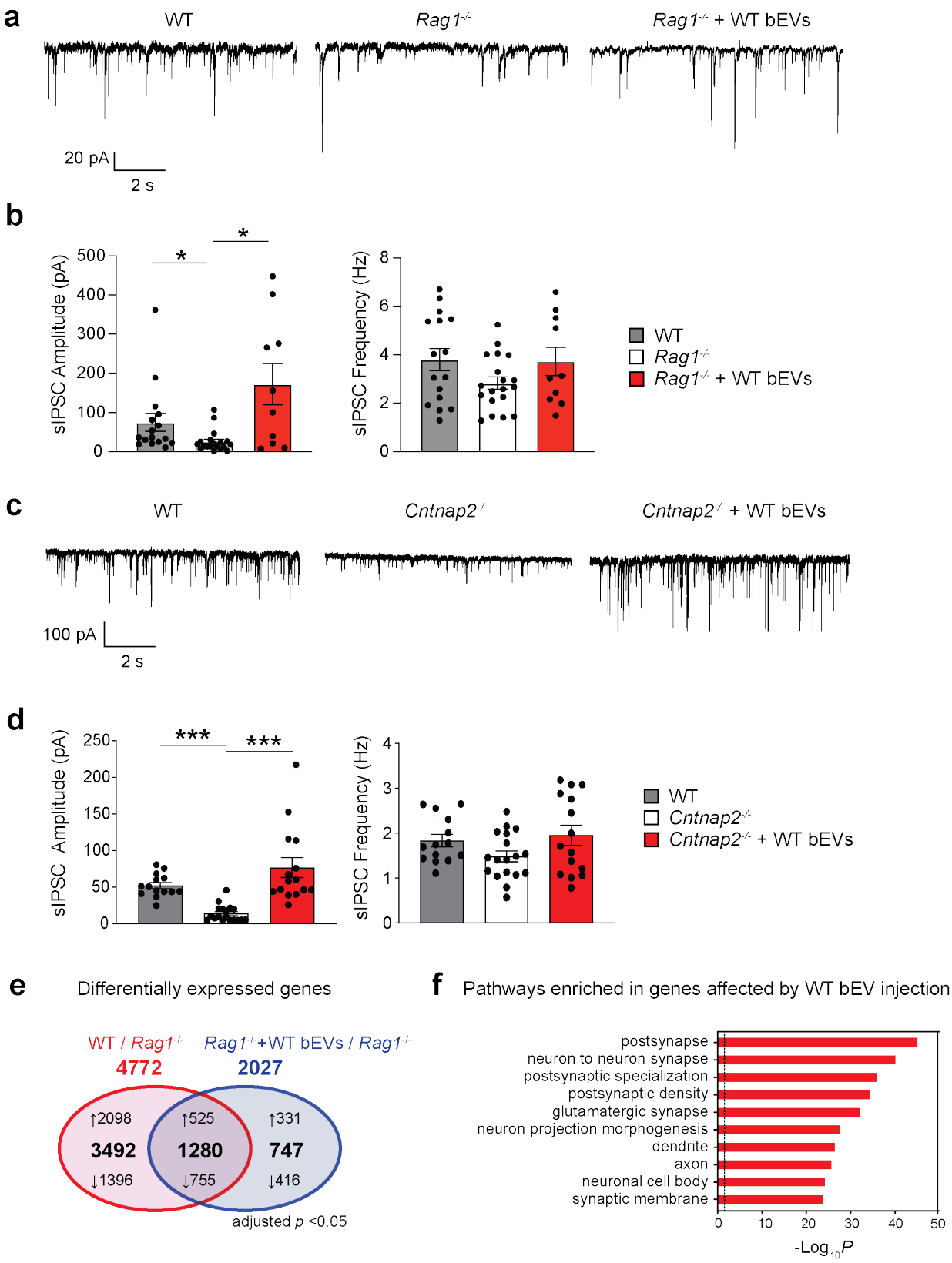
a
WT
Rag1-/-
Rag1-/- + WT bEVs
20 pA
2 s
b
sIPSC Amplitude (pA)
500
400
300
200
100
0
*
*
sIPSC Frequency (Hz)
8
6
4
2
0
WT
Rag1-/-
Rag1-/- + WT bEVs
c
WT
Cntnap2-/-
Cntnap2-/- + WT bEVs
100 pA
2 s
d
sIPSC Amplitude (pA)
250
200
150
100
50
0
***
***
sIPSC Frequency (Hz)
4
3
2
1
0
WT
Cntnap2-/-
Cntnap2-/- + WT bEVs
e
Differentially expressed genes
WT / Rag1-/-
4772
Rag1-/-+WT bEVs / Rag1-/-
2027
↑2098
3492
↓1396
↑525
1280
↓755
↑331
747
↓416
adjusted p <0.05
f
Pathways enriched in genes affected by WT bEV injection
postsynapse
neuron to neuron synapse
postsynaptic specialization
postsynaptic density
glutamatergic synapse
neuron projection morphogenesis
dendrite
axon
neuronal cell body
synaptic membrane
0
10
20
30
40
50
-Log10P

Fig. 5: WT bEVs restore impaired postsynaptic GABAergic currents in the layer V pyramidal neurons of the mPFC in *Rag1*$^{-/-}$ mice. a, Representative traces of spontaneous inhibitory postsynaptic currents (sIPSCs) in the mPFC (PrL) pyramidal neurons for WT, *Rag1*$^{-/-}$, and *Rag1*$^{-/-}$ slices exposed to WT bEVs. Voltage was clamped at -70 mV, and recordings were taken for 5 min. AP-V (50 μM) and DNQX (50 μM) were added to the bath to inhibit NMDA and AMPA receptors throughout the experiment. The temperature was set at 30 ± 1°C. **b,** Quantification of sIPSC amplitude and frequency between groups. 10-19 cells from three different mice were used for each group. Each bar represents mean ± SEM. Each dot represents one cell. **c**, Representative traces of sIPSCs in the mPFC pyramidal neurons for WT, *Cntnap2*$^{-/-}$, and *Cntnap2*$^{-/-}$ slices exposed to WT bEVs. **d,** Quantification of sIPSC amplitude and frequency between groups. 14-18 cells from three different mice were used for each group. Each bar represents mean ± SEM of recorded cells. Each dot represents one cell. **e**, Venn diagram showing the numbers of differentially expressed genes in the mPFC of *Rag1*$^{-/-}$ mice compared to WT mice and those in the mPFC of *Rag1*$^{-/-}$ mice with WT bEV injection compared to *Rag1*$^{-/-}$ mice with medium injection. WT mice, n = 3; *Rag1*$^{-/-}$ mice, n = 3*; Rag1*$^{-/-}$ mice + WT EVs, n = 3. **f,** Pathway enrichment analysis of 1280 genes whose expression were altered in opposite directions between WT vs *Rag1*$^{-/-}$ and *Rag1*$^{-/-}$ vs *Rag1*$^{-/-}$ + EV comparisons. *p<0.05, ***p<0.005. Significance was determined by one-way ANOVA and Kruskal-Walis tests with respective multiple comparison tests. See Supplementary Table 13 for the detail of statistical analysis.

Fig.6

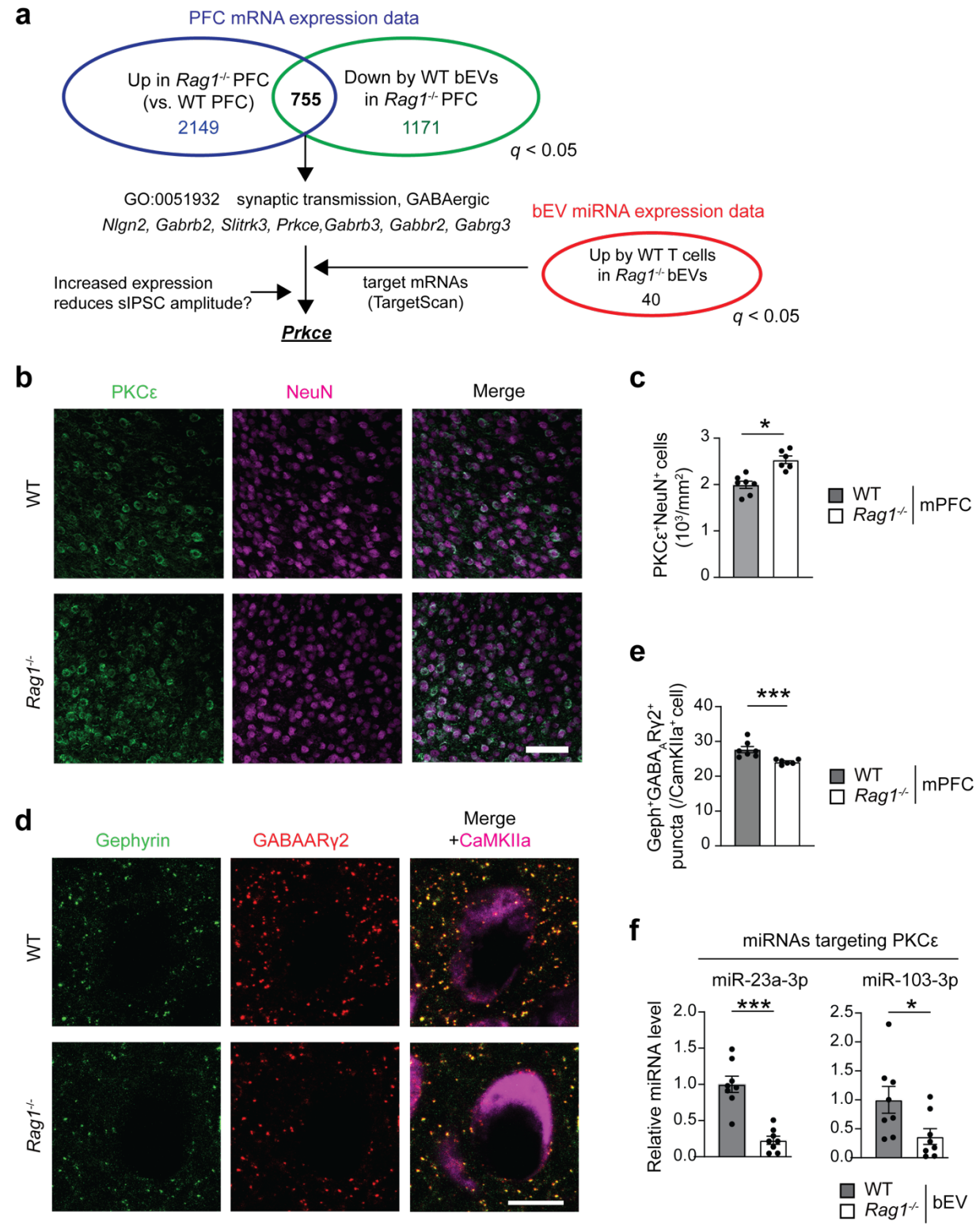
a
PFC mRNA expression data
Up in Rag1-/- PFC (vs. WT PFC)
2149
755
Down by WT bEVs in Rag1-/- PFC
1171
q < 0.05
GO:0051932 synaptic transmission, GABAergic
Nlgn2, Gabrb2, Slitrk3, Prkce, Gabrb3, Gabbr2, Gabrg3
bEV miRNA expression data
Up by WT T cells in Rag1-/- bEVs
40
q < 0.05
Increased expression reduces sIPSC amplitude?
target mRNAs (TargetScan)
Prkce
b
PKCε
NeuN
Merge
WT
Rag1-/-
c
PKCε+NeuN+ cells (10³/mm²)
*
WT
Rag1-/-
mPFC
d
Gephyrin
GABAARγ2
Merge +CaMKIIa
WT
Rag1-/-
e
Geph+GABAARγ2+ puncta (/CamKIIa+ cell)
***
WT
Rag1-/-
mPFC
f
miRNAs targeting PKCε
miR-23a-3p
miR-103-3p
Relative miRNA level
***
*
WT
Rag1-/-
bEV

Fig. 6: *Rag1*$^{-/-}$ mice show an increased expression of PKCε in the mPFC and a downregulation of its regulatory miRNAs, miR-23a-3p and miR-103-3p, in the blood EVs. **a,** Flow of data analysis to identify candidate genes responsible for GABAergic signaling changes in *Rag1*$^{-/-}$ mPFC. **b,** Representative confocal microscope images showing an enhanced neuronal PKCε immunoreactivity the mPFC of *Rag1*$^{-/-}$ mice. **c,** Quantification of PKCε^{+} neurons in the mPFC of WT and *Rag1*$^{-/-}$ mice (n = 7 per group). **d,** Representative confocal microscope images of Gephyrin and $GABA_A$Rγ2 co-localization in CaMKIIα^{+} neurons of WT and *Rag1*$^{-/-}$ mPFC. **e,** Quantification of number of overlapped puncta of Gephyrin and $GABA_A$Rγ2 in CaMKIIα^{+} neurons of WT and *Rag1*$^{-/-}$ mPFC (n = 7 per group). **f,** Expression levels of miR-23a-3p and miR-103-3p in the bEVs from WT and *Rag1*$^{-/-}$ mice (n = 8 per group). Data are shown as fold-change relative to WT data. Scale bar, 50 μm. Each bar represent mean ± SEM. Each dot represents one mouse. ns, not significant. $^{**}p$ <0.01, $^{***}p$<0.005. Significance was determined by Student's *t*-test. See Supplementary Table 13 for the detail of statistical analysis.

Fig. 7

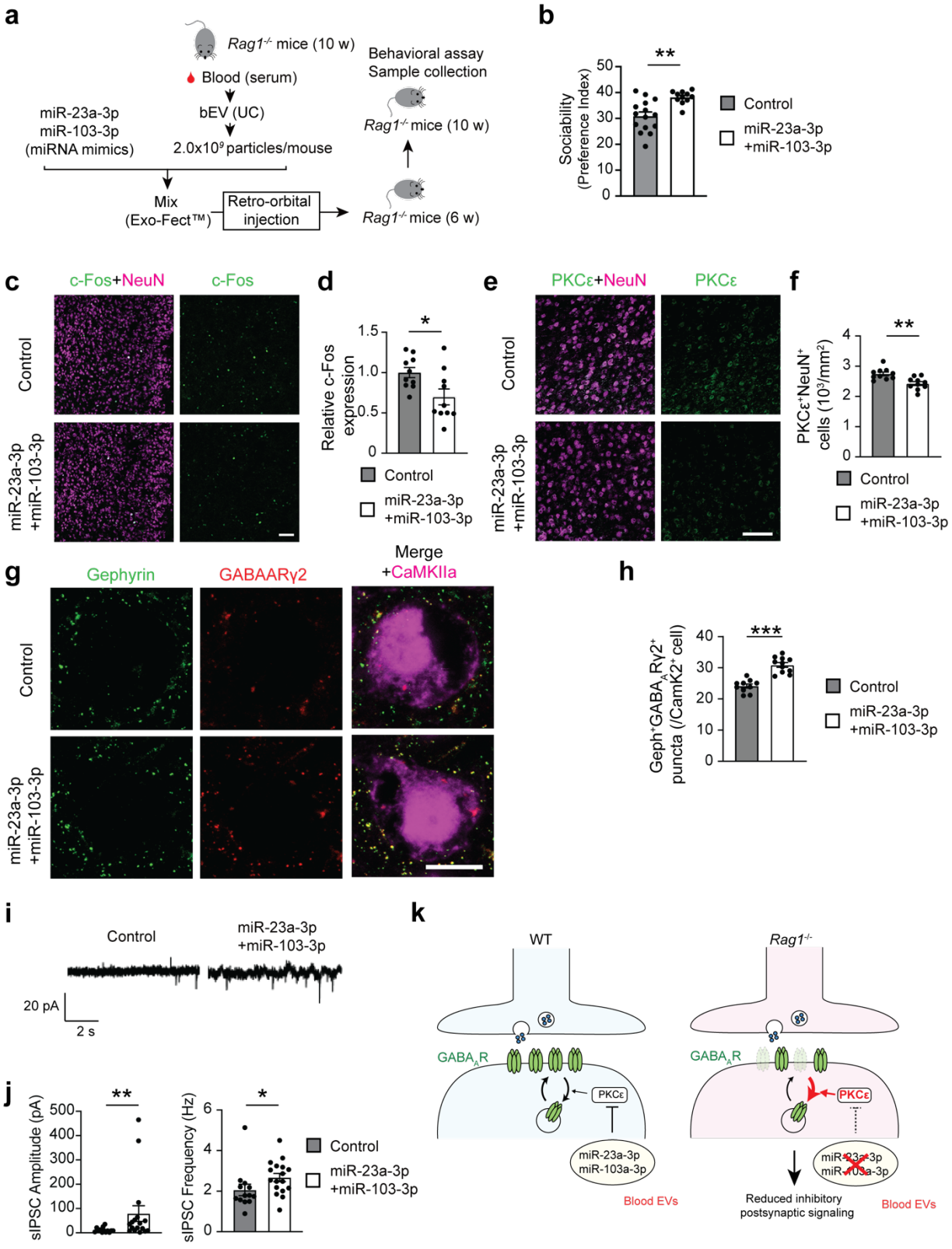
a
Rag1-/- mice (10 w)
Blood (serum)
bEV (UC)
2.0x10^9 particles/mouse
miR-23a-3p
miR-103-3p
(miRNA mimics)
Mix
(Exo-Fect™)
Retro-orbital injection
Behavioral assay
Sample collection
Rag1-/- mice (10 w)
Rag1-/- mice (6 w)
b
Sociability (Preference Index)
Control
miR-23a-3p +miR-103-3p
c
c-Fos+NeuN
c-Fos
Control
miR-23a-3p +miR-103-3p
d
Relative c-Fos expression
e
PKCε+NeuN
PKCε
f
PKCε+NeuN+ cells (10³/mm²)
g
Gephyrin
GABAARγ2
Merge +CaMKIIa
h
Geph+GABAARγ2+ puncta (/CamK2+ cell)
i
Control
miR-23a-3p +miR-103-3p
20 pA
2 s
j
sIPSC Amplitude (pA)
sIPSC Frequency (Hz)
k
WT
Rag1-/-
GABAAR
PKCε
miR-23a-3p
miR-103a-3p
Blood EVs
Reduced inhibitory postsynaptic signaling

Fig. 7: Supplementation of miR-23a-3p and miR-103-3p to *Rag1*$^{-/-}$ bEVs affects the mPFC molecular and functional changes in *Rag1*$^{-/-}$ mice and enhances their sociability. a, Experimental outline of bEV collection, miRNA mimics loading, intravenous injection, and subsequent behavioral assay. **b,** Sociability data of *Rag1*$^{-/-}$ mice administered with negative control miRNA mimics (control mimics) and miRNA mimics for miR-23a-3p and miR-103-3p (miR-23a-3p + miR-103-3p mimics). Control, n = 15; miR-23a-3p + miR-103-3p, n = 11. **c,** Representative confocal microscope images of neuronal c-Fos expression in the mPFC of *Rag1*$^{-/-}$ mice administered with control and miR-23a-3p + miR-103-3p mimics (n = 10 mice per group). **d,** Quantification of c-Fos^{+} neurons in the mPFC of WT and *Rag1*$^{-/-}$ mice (n = 7 per group). **e,** Representative confocal microscope images of neuronal PKCε expression in the mPFC of *Rag1*$^{-/-}$ mice administered with control and miR-23a-3p + miR-103-3p mimics (n = 10 mice per group). **f,** Quantification of PKCε^{+} neurons in the mPFC of WT and *Rag1*$^{-/-}$ mice (n = 10 per group). **g,** Representative confocal microscope images of neuronal Gephyrin and $GABA_A$ expression in CaMKIIα^{+} cells in the mPFC of *Rag1*$^{-/-}$ mice administered with control and miR-23a-3p + miR-103-3p mimics. **h,** Quantification of number of Gephyrin and GABA-A puncta in CaMKIIα^{+} in the mPFC of WT and *Rag1*$^{-/-}$ mice (n = 10 per group). **i,** Representative traces of sIPSCs of the mPFC layer V neurons in brain slices from *Rag1*$^{-/-}$ mice administered with control and miR-23a-3p + miR-103-3p mimics. **j,** Quantification data of sIPSC amplitude and frequency changes by miR-23a-3p + miR-103-3p mimics in *Rag1*$^{-/-}$ mice (aggregated data from n = 3 mice per group). **k,** Graphical summary of mechanism. Circulating EV miRNAs, including miiR-23a-3p and miR-103-3p in circulating EVs inhibits the expression of PKCε in mPFC neurons increasing synaptic $GABA_A$ receptor localization, and enhancing inhibitory postsynaptic signaling. Scale bars, 50 μm (**c** and **e**) and 10 μm (**i**). Each bar represent mean ± SEM. ns, not significant. *p<0.05, **p <0.01, and ***p<0.005. Significance was determined by Student's *t*-test. See Supplementary Table 13 for the detail of statistical analysis.

Fig. 8

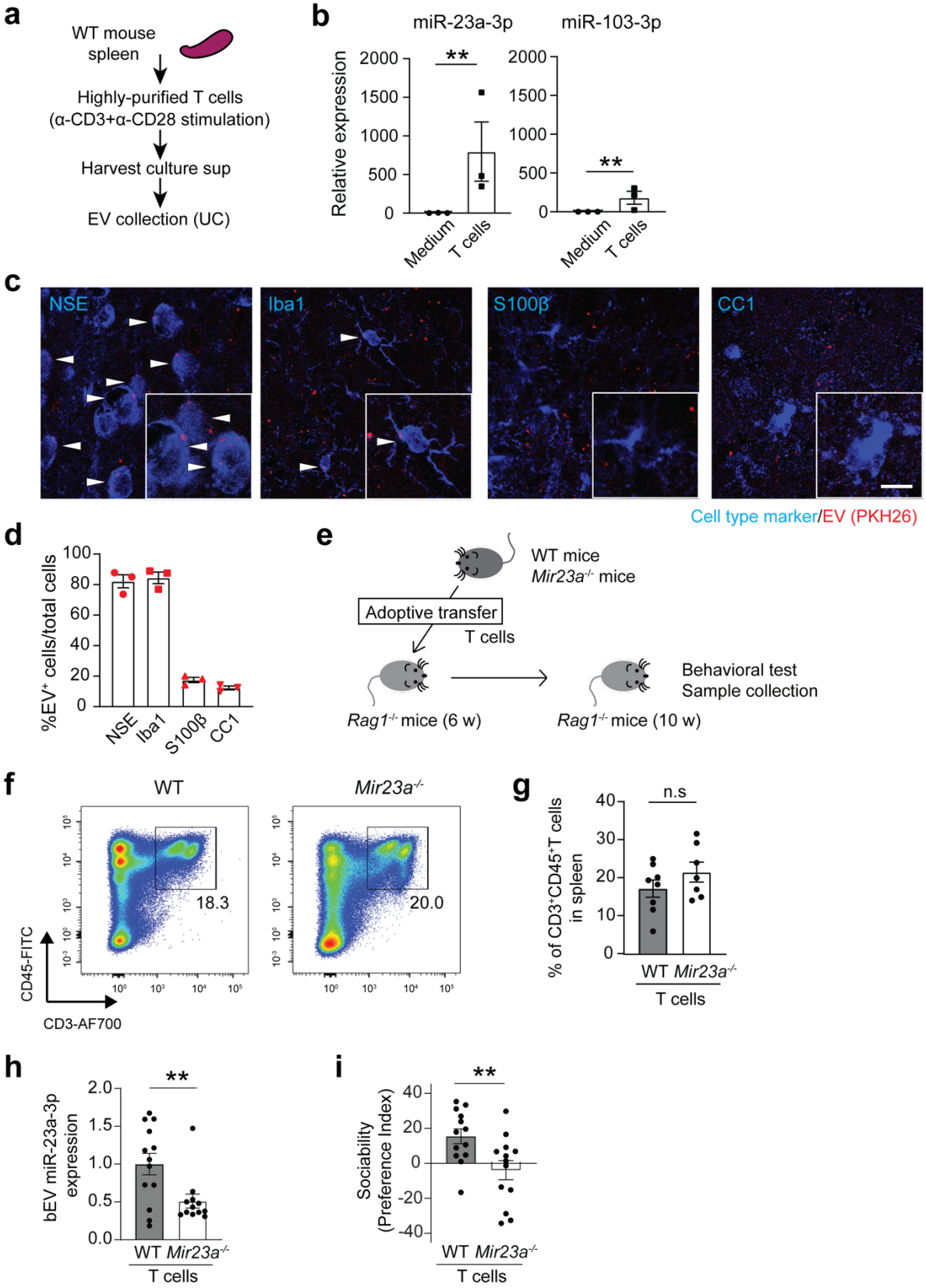
a
WT mouse spleen
Highly-purified T cells (α-CD3+α-CD28 stimulation)
Harvest culture sup
EV collection (UC)
b
miR-23a-3p
miR-103-3p
Relative expression
2000
1500
1000
500
0
**
Medium
T cells
c
NSE
Iba1
S100β
CC1
Cell type marker/EV (PKH26)
d
%EV+ cells/total cells
100
80
60
40
20
0
NSE
Iba1
S100β
CC1
e
WT mice
Mir23a-/- mice
Adoptive transfer
T cells
Rag1-/- mice (6 w)
Rag1-/- mice (10 w)
Behavioral test
Sample collection
f
WT
Mir23a-/-
18.3
20.0
CD45-FITC
CD3-AF700
g
% of CD3+CD45+T cells in spleen
n.s
40
30
20
10
0
WT
Mir23a-/-
T cells
h
bEV miR-23a-3p expression
2.0
1.5
1.0
0.5
0.0
**
WT
Mir23a-/-
T cells
i
Sociability (Preference Index)
40
20
0
-20
-40
**
WT
Mir23a-/-
T cells

Fig. 8: T cell-derived miR-23a-3p contributes to circulating bEVs and sociability.

a, Experimental outline of splenocyte collection, primary T cell culture, and subsequent EV collection from T cell culture supernatants. **b,** Levels of miR-23a-3p and miR-103-3p expression in T cell-derived EVs (n = 3 biologically independent experiments). **c**, Representative confocal microscope images of PKH26-labeled T cell-derived EVs (red) colocalization with neurons (NSE^+ cells) and microglia ($Iba1^+$ cells), but not astrocytes ($S100\beta^+$ cells) or oligodendrocytes ($CC1^+$ cells) in the mPFC of *Rag1*$^{-/-}$ mice. EV^+ cells are indicated by white arrowheads. Scale bar, 10 μm. **d,** Quantification data of T cell-derived EV co-localization with specific brain cell types (n = 3 mice). **e**, Experimental outline of adoptive transfer/serum injection and subsequent behavioral assay. **f**, Representative flow cytometry data showing the comparable reconstitution of T cells in *Rag1*$^{-/-}$ mice by adoptively transferred WT and *Mir23a*$^{-/-}$ T cells. **g**, Quantification of WT and *Mir23a*$^{-/-}$ T cell reconstitution in *Rag1*$^{-/-}$ mice (n = 8 for WT and n = 7 for *Mir23a*$^{-/-}$ T cell reconstitution group). **h**, miR-23a-3p levels in EVs from *Rag1*$^{-/-}$ mice receiving WT and *Mir23a*$^{-/-}$ T cells (n = 13 mice per group). **i**, Sociability of *Rag1*$^{-/-}$ mice receiving WT and *Mir23a*$^{-/-}$ T cells (n = 13 each). Each bar represents mean ± SEM. Each dot represents one mouse. $^*p<0.05$, $^{**}p<0.01$, and $^{***}p<0.005$. n.s., not significant. Significance was determined by Student's *t*-test. See Supplementary Table 13 for the detail of statistical analysis.